NANOPOWDER NICKEL ALUMINATE FOR BENZOTHIOPHENE ADSORPTION FROM DODECANE

A Thesis
Submitted to
The Academic Faculty

By

John Daniel Berrigan

In partial fulfillment
Of the Requirements for the Degree
Master of Sciences in Materials Science and Engineering

Georgia Institute of Technology
Atlanta, GA

December 2008

Nanopowder Nickel Aluminate for Benzothiophene Adsorption from Dodecane

Approved by:

Dr. W. B. Carter, Advisor
School of Materials Science and Engineering
Georgia Institute of Technology

Dr. Ganesh Venugopal
Research Scientist
nGimat, Inc.

Dr. Joseph K. Cochran
School of Materials Science and Engineering
Georgia Institute of Technology

Date Approved:
October 31, 2008

ACKNOWLEDGEMENTS

I'd like to thank my parents for their life-long support and guidance. Their encouragement and love has helped me achieve more than I ever could have on my own. I am also grateful for the support from Dr. Tom Sanders. If it were not for him and his love of college basketball, my enrollment at Georgia Tech would have never become a reality, and none of this would have been possible. I'd like to thank Dr. Brent Carter as well for his guidance and instruction throughout this research. He is a wonderful teacher and mentor, and always available to lend help. Finally, Dr. Andrew Hunt and everyone at nGimat deserve lots of thanks for their help. Thank you for allowing me to work at your company, and thank you for your patience and assistance from start to finish.

TABLE OF CONTENTS

LIST OF TABLES

LIST OF FIGURES

SUMMARY

To simplify fuel logistics, the military needs to replace diesel and gasoline fuels used by ground and support vehicles with JP-8 jet fuel. JP-8 contains 300 to 3,000 ppm of sulfur despite state-of-the-art hydrodesulfurization (HDS) treatments. Sulfur concentrations of this magnitude are harmful to both the environment and the performance of catalysts in catalytic converters. If military ground and support vehicles are to utilize JP-8 fuel without fouling the catalytic converters required by the Environmental Protection Agency (EPA), sulfur content of JP-8 must be reduced to less than 15 ppm. Achieving this goal requires a method that targets the sterically-hindered and electronically delocalized sulfur atoms found in thiophenic compounds left behind by HDS. While HDS could be ramped up to meet the demand of ultra-low sulfur JP-8, the high temperatures and pressures of hydrogen needed make the process costly and severely degrade the octane rating of the fuel. As a result, the military needs an alternative to HDS that is both cost effective and practical for use in the field.

Low temperature adsorption of thiophenic compounds is an effective sulfur removal technique that has traditionally relied on metal ion impregnated zeolite materials. However, zeolites may not be the ideal material due to their small pore sizes and limitations on metal loading. Combustion chemical vapor condensation (CCVC) is a process whereby an oxide support and an active metal surface are synthesized in a single step. In addition, CCVC materials have both a high surface area and high metal loading per unit mass, making them an attractive alternative to zeolite supported catalysts.

The use of adsorbents in the ultra-deep desulfurization of fuels presents its own challenges. Due to the molecular structure of thiophenic compounds, the sulfur atom is largely inaccessible and its electrons delocalized. Consequently, active metal adsorbents require an open d-electron shell that is able to bind with the thiophene through π-complexation. Nanopowders created via CCVC are typically oxides. Therefore, the active metal sites will need to be reduced from their oxide form at high temperatures under hydrogen, and a loss of surface area due to sintering is expected after use and regeneration cycling.

This project focuses on the use of $NiAl_2O_4$ nanopowders for use as a benzothiopene adsorbent in dodecane. The powder adsorbent is formed into pellets before being placed into a fixed-bed reactor. After a H_2 reduction, the adsorbent is then exposed to a constant flow of a model fuel composed of benzothiophene in dodecane (300 ppmw S). The effluent fuel is regularly collected and the sulfur concentration measured using gas chromatography. Regeneration of the spent adsorbent was attempted using heat treatments under flow of either air or hydrogen. Finally, the reduction and adsorption conditions were optimized. The phase and surface compositions of the powders were measured using x-ray diffraction and x-ray photoelectron spectroscopy, respectively. Transmission electron microscopy and surface area analysis was used to characterize average particle size and surface area. $NiAl_2O_4$ was able to clean 3.4 ml of model fuel to less than 15 ppmw S per gram of adsorbent. The used adsorbent regained 40% of its original capacity after air regeneration.

CHAPTER 1

INTRODUCTION

Attention to the deep desulfurization of fuels has grown due to the increasing concern over the harmful effects of sulfur on both the environment and catalytic converters. Motivating demand further are fuel cells where concentrations of less than 1 ppmw S poison catalysts.[1] In response, the United States Environmental Protection Agency (EPA) and other foreign governments are implementing more stringent regulations concerning sulfur in fuels. In 2006, the EPA began requiring refineries to reduce sulfur concentrations to 30 ppmw in gasoline and to 15 ppmw in diesel.[2, 3] It stands to reason that JP-8 is the next likely target for government regulation as the typical sulfur concentration JP-8 is close to 500 ppmw.[4, 5]

Hydrodesulfurization (HDS) is the primary desulfurization process used worldwide, but involves passing the input fuel over a catalyst at high temperatures (>300˚C) and pressures (20-100 atm H_2).[1-4] In HDS, sulfur compounds chemically adsorb to catalytic sites where carbon-sulfur bonds are cleaved to form H_2S and aliphatic hydrocarbons.[6] Compounds such as thiophene, benzothiophene, and dibenzothiophene are relatively non-reactive in HDS due the combination of electron delocalization around the sulfur atom and steric hinderence, which physically prevents the sulfur atom from interacting with the catalyst.[2] As a result, achieving EPA Tier II standards with conventional HDS processing requires an increase either in the volume of the catalyst bed or the catalyst activity by more than a factor of three.[1, 2, 4] Moreover, both the demand for crude oil and its average sulfur content are increasing, while its quality, measured by API gravity, is

decreasing (Table 1).[4] Poor input fuel quality is worsened by the high temperatures and pressures of H_2 used in HDS, and further reduce octane and cetane ratings. These issues have led to investigations of alternative methods of producing ultralow-sulfur fuels either by selective adsorption,[6-9] oxidation,[10, 11] or biodesulfurization.[12]

Table 1. Average properties of crude oils refined in the US during 1981-2001 and US and world petroleum consumption during 1981-2001. [4]

Property	Year		
	1981	1991	2001
Total crude oil refined in US (million barrel/day)	12.47	13.30	15.13
Average sulfur content of crude oil refined in US (wt.% based on sulfur)	0.89	1.13	1.42
API gravity of crude oil refined in US (° API)	33.74	31.64	30.49
Total petroleum products supplied in the US including imported crude and products (million barrel/day)	16.06	16.71	19.59
Total worldwide petroleum consumption (million barrel/day)	60.90	66.72	77.12

Selective adsorption is one of the more attractive options for desulfurization because it can be achieved under lower temperatures and ambient pressure. As a consequence, it can easily be integrated into the fuel system of a refinery or vehicle. Various adsorbent materials that reduce sulfur concentrations to sub-ppm levels include metal oxides,[13] active carbon and carbon nanotubes,[14, 15] clays,[16] and zeolites.[17, 18] In literature, copper ion-exchanged zeolites demonstrate superior capacity due to their high surface areas, selectivity, and ability to π-complex with thiophenic compounds.[19] Other studies have reported significant sulfur adsorption using nickel or zinc ion-exchanged zeolites.[9]

The work presented is motivated by the desire of the United States Air Force to replace diesel and gasoline with JP-8 to simplify fuel logistics. The sulfur content in JP-8 causes harm to engines, poison catalytic converters, and leads to the violation of EPA regulations if used in ground vehicles.[1, 4]

The objective of this project is to investigate nanopowder materials created via combustion chemical vapor condensation (CCVC) for use as a high capacity, regenerable adsorbent that removes benzothiophene to sub-ppm concentrations. CCVC begins with organometallic pre-cursor solutions that are atomized and ignited to create nanocrystalline oxide powders. It is an economical and flexible technique for synthesizing large quantities of ceramic powders.

Pellets of $NiAl_2O_4$ were tested in a fixed-bed reactor after hydrogen reduction. In the experiment, a model fuel comprised of benzothiophene in dodecane (300 ppmw S) is passed over the adsorbent at a constant rate. Regular collections of the effluent fuel were sampled and sulfur content was measured using gas chromatography. The measured sulfur concentrations were used to construct breakthrough curves which show the specific sulfur capacity of the adsorbent. The dependence of sulfur capacity on the length and temperature of H_2 reduction as well as reactor temperature was tested to optimize the process. After the adsorbent was saturated by the sulfur, it was regenerated using high temperature treatments under either H_2 or air atmospheres.

This thesis begins with a review of the published literature on HDS, the development of sulfur adsorbents, and the use of nanomaterials as adsorbents. Next, an overview of the processing route along with an explanation of the selected materials, model fuels, experimental procedures and testing apparatus are presented. The adsorption breakthrough capacities and characterization of the materials tested are presented. Also, the results of optimization and regeneration experiments are discussed. Finally, conclusions are drawn and recommendations for future work proposed.

CHAPTER 2

LITERATURE REVIEW

In this section, the literature relevant to the ultra-deep desulfurization of fuels is summarized. Emphasis is placed on desulfurization via zeolites and nanopowder adsorbents.

2.1 Foundational Work in Fuel Desulfurization

Desulfurization via HDS has been in use since World War II when it was a means of supplementing aviation fuel base stocks.[20] Major development began in the early 1940's when Byrns et al. established that HDS improved the susceptibility of fuels to tetraethyllead.[21] Later it was discovered that desulfurization decreased the octane number of fuels by 4 to 8 units.[22] The objective of subsequent research focused on maximizing the level of desulfurization while minimizing the reduction of the unleaded octane number of the fuel.

Metal sulfide catalysts such as MoS_2 showed a marked improvement in selectivity, and eventually HDS became dominated by these sulfided catalysts.[21] The improved selectivity is explained by the rim-edge model, which was developed later by Daage and Chianelli for MoS_2 crystals. MoS_2 is comprised of a layered structure that can be modeled as a stack of several discs.[23] The top and bottom discs supply rim sites for adsorption while the discs in-between yield edge sites. High temperature hydrogen flow creates sulfur atom vacancies on both rim and edge sites. Sulfur-containing species in the

fuel then chemically adsorb to the vacancy sites. Once adsorbed, the C-S bonds are cleaved and replaced by hydrogen, leaving behind a sulfur atom to fill the vacancy and an aliphatic hydrocarbon.[23]

Table 2. Reference data showing typical reactivity pattern observed in hydrodesulfurization catalysis.[24, 25]

Reactant	Structure	Pseudo-first-order rate k (L/g cat)	Rate constant $(min^{-1})^{***}$
Thiophene		$1.38 \times 10^{-3*}$	
Benzothiophene		$8.11 \times 10^{-4*}$	>0.20 (CoMo) >0.20 (NiMo)
Dibenzothiophene	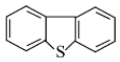	$6.11 \times 10^{-5*}$	
Benzo[*b*]naphtho-[2,3-d] thiophene	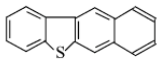	$1.61 \times 10^{-4*}$	
Dibenzothiophene	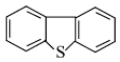	$7.38 \times 10^{-5**}$	0.058 (CoMo) 0.057 (NiMo)
4-Methyldibenzothiophene	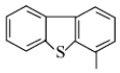	$6.64 \times 10^{-6**}$	0.018 (CoMo) 0.020 (NiMo)
4,6-Dimethyldibenzothiophene	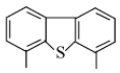	$4.92 \times 10^{-6**}$	0.006 (CoMo) 0.008 (NiMo)
2,8-Dimethyldibenzothiophene	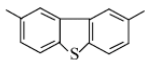	$6.72 \times 10^{-5**}$	
3,7-Dimehyldibenzothiophene	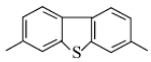	$3.53 \times 10^{-5**}$	

The original data * appear in reference [26] and the data ** appear in reference [27]. The data *** are from reference [28].

The direct, chemical interaction with the sulfur atom means that molecules with accessible sulfur atoms such as thiols, sulfides, and disulfides are easily removed via HDS. However, larger organosulfur molecules such as dibenzothiophene and 3,7-dimethyldibenzothiphene are more difficult to remove due to steric hinderance and increased electron delocalization. Girgis et al. compiled the pseudo-first-order reaction rates that are complied in Table 2.[25]

The sulfur compounds left behind after HDS in the three major transportation fuels – commercial gasoline, diesel and jet fuel – were analyzed by Song et al. via gas chromatography with a flame photometric detector (GC-FPD).[2] The chromatogram, shown in figure 1, reveals five major sulfur compounds in gasoline: thiophene, 2-methylthiophene, 3-methylthiophene, 2,4-dimethylthiophene and benzothiophenes. In JP-8 the major sulfur-containing compounds are dimethylbenzothiophene and trimethylbenzothiophenes. No benzothiophenes or dibenzothiophenes were detected. Sulfur compounds in commercial diesel were more complex and included alkyl benzothiophenes and dibenzothiophenes with methyl groups at the 4- and 6-positions. From figure 1 it is apparent that as the fuels become higher in boiling point, the sulfur compounds remaining after HDS treatment become larger in ring size and higher in number of substitutes.[23, 29]

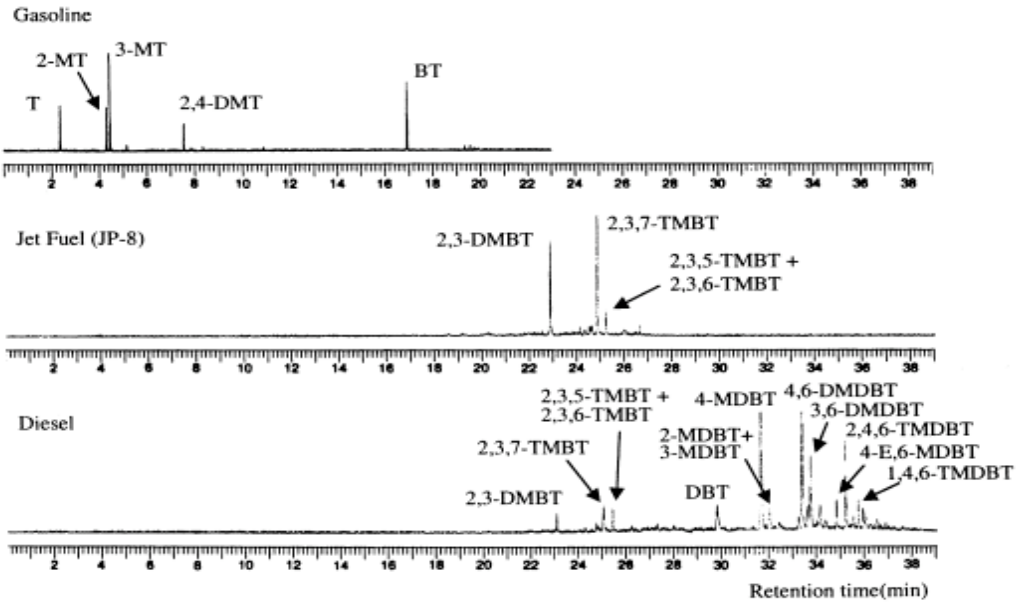

Fig. 1: GC-FPD chromatograms collected by Song et al. showing typical compounds left behind by HDS in gasoline, jet fuel and diesel.[4]

In summary, the investigation of alternative desulfurization methods to HDS stems from the following issues: (1) the desire remove larger organosulfur compounds from feed stocks without degrading the octane rating of the fuel; (2) the increasing hydrogen demand and deficits;[30] (3) the tightening of government sulfur regulations.

2.2 Adsorptive Desulfurization via Zeolites

Among the various alternative techniques, adsorptive desulfurization is considered to be a promising approach due to its negligible demands on processing conditions and reactor design. An ideal adsorbent has the following qualities: (1) significant adsorption capacity at mild temperature and pressure, (2) regeneration ability, (3) low cost, and (4) high selectivity towards all sulfur containing compounds.[31]

Over subsequent decades, many reports have investigated adsorptive materials such as zeolites, [17] activated carbon,[32] and nanopowders.[33] All of these materials have shown some adsorption capacity in model or real fuels due either to physical adsorption or chemical complexation between sulfur molecules and the adsorbent. In 1994 Salem et al. compared the sorption capacities of zeolites 5A and 13X to activated carbon in a solution of naptha and 50 ppm sulfur at 20°C.[34] The data indicate that 13X is more effective at lower sulfur concentrations, but activated carbon performs better once sulfur concentrations become greater than 25 ppm. Zeolite 5A did not show any desulfurization ability. After further study, Salem concluded that at higher adsorption temperatures and sulfur concentrations of 550 ppm, zeolites 13X showed less capacity, possibly due to competition amongst sulfur compounds, olefins, and aromatics.[35]

Despite its better performance at high sulfur concentrations, the inherent properties of the carbon surface limit its use. Due to its hydrophobic surface, carbonecous materials tend to not be very selective and adsorb aromatic compounds in significant amounts.[36] These aromatics are the key component for octane number; as a result, more work has gone into developing zeolites and improving their selectivity and capacity.

Both zeolites and activated carbons behave as high surface area molecular traps, but as mentioned before, the carbon surface adsorbs important aromatics from the fuel. Zeolites can be designed synthetically with a uniform, well-defined pore structure, that allows for the material to selectively adsorb molecules on the basis of size, configuration, polarity, and other physical characteristics.[37] The shapes and dimensions of pores in the material cause molecules that diffuse in to have difficulty diffusing out. As a result, incoming molecules are retained inside the microporous structure. Weitkamp et al. investigated ZSM-5 zeolite in a fixed-bed reactor and found that thiophene adsorbed more selectively than benzene.[38] The result led to further studies involving zeolites materials.

Building on the initial studies of thiophenic compounds over 13X and other zeolites, Ng et al. expanded their study to include NaY, USY, and HY.[39] As shown in table 3, NaY is the most effective adsorbent for thiophenes in hexadecane in each case. Its performance is also comparable to activated carbon. For thiophene adsorption, capacity follows: NaY > HY ~ USY ~ 13X. HY zeolite has a higher sorption capacity at low thiophene concentrations, which is attributed to the direct interaction of the acidic sites with the thiophene. Thermal desorption analysis shows the degree of acidity of the zeolites to be:

USY > HY > 13X > NaY. These results demonstrate that increasing the acidity of the material reduces the saturation sorption capacity of the zeolites. There is also a systematic decrease in adsorption capacity with increasing size of the sulfur containing molecules. This behavior is similar to HDS and is also an indicator that thiophenic compounds are chemically adsorbed by each of the zeolites. These results are significant because previous studies involved only physical adsorption of thiophenic compounds.

Table 3. Adsorption data for different adsorbents.[39]

Sorbent and sulfur compounds	Sulfur removal capacity* (mmol S/g-Sorbent)
NaY	
Thiophene/*n*-$C_{16}H_{34}$	1.89
Benzothiophene/*n*-$C_{16}H_{34}$	1.40
Dibenzothiophene/*n*-$C_{16}H_{34}$	1.00
USY	
Thiophene/*n*-$C_{16}H_{34}$	1.48
Dibenzothiophene/n- $C_{16}H_{34}$	0.70
HY	
Thiophene/*n*-$C_{16}H_{34}$	1.50
Dibenzothiophene/*n*-$C_{16}H_{34}$	0.55
13X	
Thiophene/*n*-$C_{16}H_{34}$	1.45
Dibenzothiophene/*n*- $C_{16}H_{34}$	0.60

* Determined from equilibrium adsorption at 55°C.

To confirm that NaY zeolites were selectively adsorbing thiophene, the heats of adsorption for the different sulfur compounds were measured by flow calorimetry and plotted as a function of adsorption capacity per gram of adsorbent (fig. 2).[39] The linear relationship suggests a similar mechanism of interaction between the sulfur molecules and the zeolites regardless of compound. The average heat of adsorption was calculated from the slope to be 20.9 kJ/mol of S. Since it is important for sulfur sorbents to not just

have a high capacity but be easily regenerated, the heat of adsorption is an important design parameter.

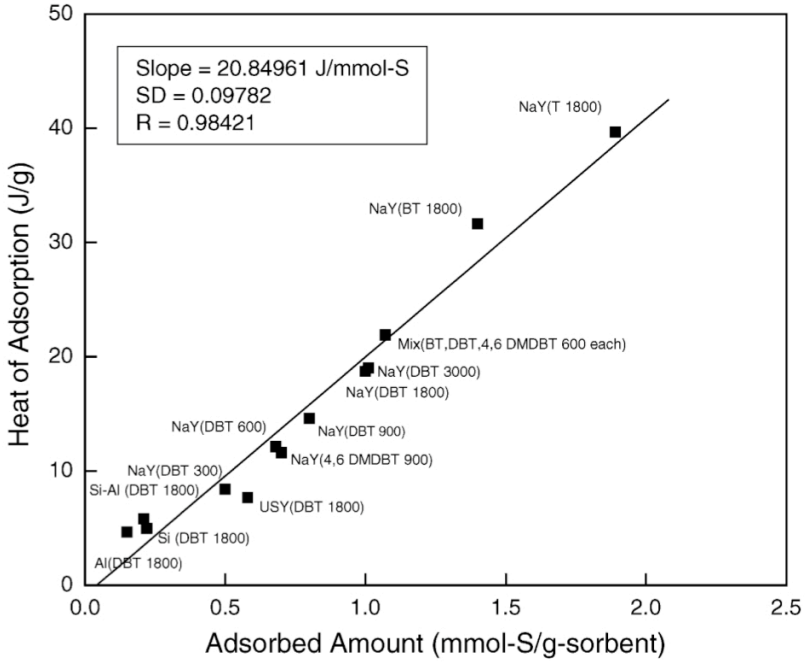

Fig. 2: A study of the heat of adsorption of thiophene over various zeolite adsorbents.[39]

To further increase the capacity and selectivity of zeolites adsorbents, liquid and vapor phase ion exchanged zeolites were developed. In 2002, Takahashi et al. reported new zeolite sorbents prepared by a wet ion exchange of NaY zeolites.[15] NaY zeolites were impregnated with an aqueous solution of $Cu(NO_3)_2$, then autoreduced to Cu^+-Y in a He atmosphere for 1 hour at 450°C. Ag^+-Y ion exchanged zeolites adsorbents were synthesized in a similar fashion. Both Ag^+-Y and Cu^+-Y adsorbed a significant amount of thiophene 0.92 molecules/Cu^+ and 0.42 molecules/Ag^+, which were significantly greater than Na-ZSM-5 zeolites, activated carbon, NaY and modified alumina.

To understand the mechanism behind these high capacity adsorbents, molecular orbital calculations were employed. The increased capacity was shown to be due to π-complexation between Cu^+ cations and the aromatic rings of the thiophene.[19] Cu^+ ions have an electron configuration of $1s^2 2s^2 2p^6 3s^2 3p^6 3d^{10} 4s^0$ and when the thiophene molecules adsorb, the cations form σ-bonds with their empty s-orbital. Additionally, their d-orbitals back-donate electron density to the anti-bonding π-orbitals (π^*) of the sulfur rings (fig. 3). Additionally, molecular orbital simulations showed that π-complexation is more favorable with sulfur containing molecules than other non-sulfur containing aromatics.

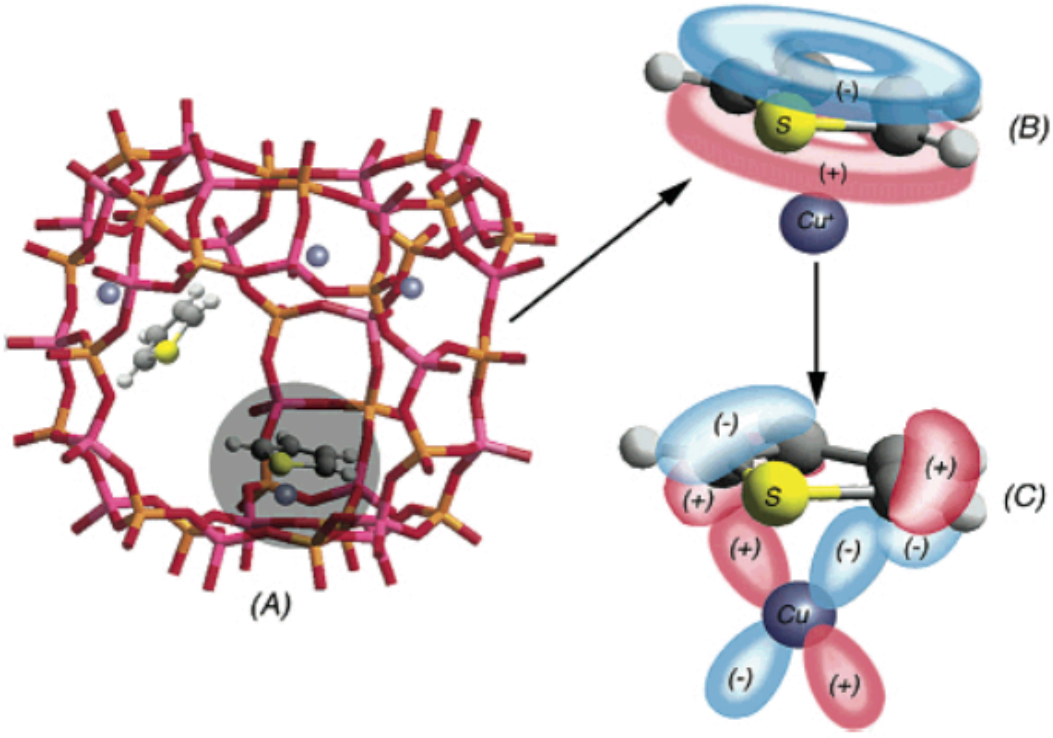

Fig. 3: Faujasite supercage with copper ions occupying 6-ring windows sites (A); σ-donation of π-electrons of thiophene to the 4s orbital of Cu^+ (B); d-π^* back-donation of electrons from 3d orbitals of Cu^+ to π^* orbitals of thiophene (C).[19]

After Cu^{+}-Y zeolites displayed significant adsorptive properties, researchers began investigating other transition metal ions and other ion exchange methods. Hernández-Maldonado et al. compared the performance of faujasite type zeolites ion exchanged with Cu^{+}, Ni^{2+} or Zn^{2+} cations via liquid phase ion exchange (LPIE), vapor phase ion exchange (VPIE) and solid-state ion exchange (SSIE).[9] Fixed bed adsorption tests revealed the order of performance to decreases as follows: Cu^{+}-Y (VPIE) > Ni^{2+}-Y (SSIE) > Ni^{2+}-X (LPIE) > Zn^{2+}-X (LPIE) > Zn^{2+}-Y (LPIE).

The explaination behind the results begins with the processing methods. LPIE is limited by three factors: (1) the selectivity of the zeolites for the new cationic species introduced into the framework, (2) passage of solvated cations through the zeolites pores, and (3) hydrolysis of the cation species in the aqueous solution. Moreover, particular zeolites' framework and cation combinations at increasing process temperature can cause a collapse of the zeolites framework. Both VPIE and SSIE zeolites will not have issues with collapsing and are able to completely ion exchange, thereby leading to their increased performance.

Comparing the performance of the cations, Ni^{2+}-zeolites were slightly less active and therefore removed less sulfur at breakthrough. However, they are more stable under oxidizing conditions than Cu^{+}-zeolites, and their activation consisted of a single step without hydrogen or inert gas. Zn^{2+}-zeolites showed the lowest capacity despite being highly loaded with cations; therefore it is assumed that Zn^{2+} ions do not undergo strong π-complexation with thiophenic compounds.[9]

Since these adsorbents are based on the chemical reaction of a reduced metal cation, the presence of oxygenates and moisture in the fuel severely diminishes performance. Li et al. added 5000 ppm of water to the feed fuel, which decrease performance of Ni^{2+}-Y zeolites by 65%.[40] Oxygenates such as MTBE and ethanol that are blended into fuels during the refining process also diminish capacity. The Cu^{+}-Y zeolites show a 90% decrease in breakthrough capacity when a model fuel containing 5% ethanol is passed over the sorbent. The result is attributed to stronger adsorption energy of ethanol with the sorbent than that of thiophene. The addition of 300 ppmw H_2O decreased the sorption capacity in a similar amount as the 5% ethanol treatment. Cu^{+} ions are not stable in the presence of moisture and are easily converted into Cu^{2+} and Cu^{0} that do not undergo π-complexation.

Regenerating Cu^{+}-Y zeolites required an air treatment at 350ºC followed by autoreduction.[41] The regenerated adsorbent regained 85% of its original capacity. Ni^{2+}-Y and Zn^{2+}-Y adsorbents were regenerated by the single treatment in air at 350ºC.

2.3 Nanopowder Adsorbents

Currently, research of zeolites for sulfur adsorption has dominated the field, and while zeolites offer high capacities, selectivity and regenerability, investigations into other materials such as nanopowders are severely lacking. Significant advancements have been made in the area of nanopowder adsorbents for the removal of sulfur from fuels.

It has been demonstrated that a host of materials' properties depend on the size of the particles in the nanoscale regime. Band gaps change, melting points decrease, and surfaces become more reactive.[42] The entire field of nanoscience has developed as a result, and opened an almost infinite number of possible applications, including adsorption and catalysis.

The nanoparticle regime lies between the classic fields of chemistry (between 0.5 to 1 or 2 nm) and solid-state physics (10 nm up to bulk). The different chemical and physical properties stem from a substantial delocalization of valence electrons that varies with size. Important to adsorption is the material surface chemistry. In spherical nanoparticles of 3 nm in diameter, 50% of the atoms are on the surface – as shown in figure 4. This large surface to bulk atom ratio allows for the possibility of manipulating bulk properties by surface effects and allowing near stoichiometric reaction chemistry.

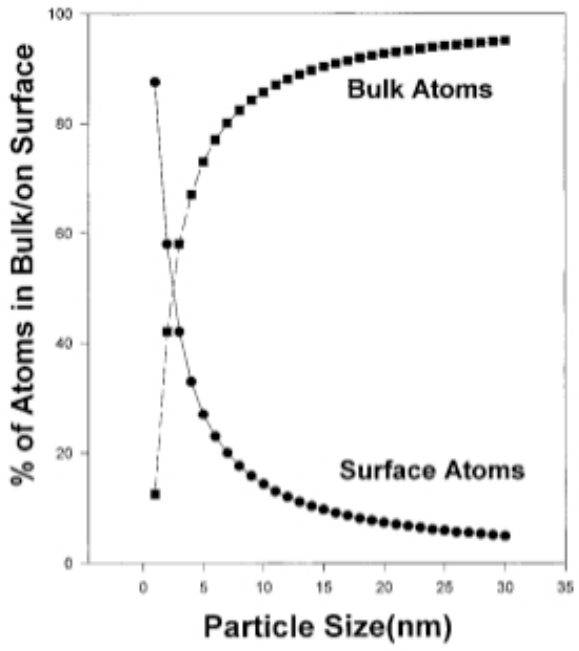

Fig. 4: Calculated surface to bulk ratios for solid metal particles versus size.[38]

In 2005, Jeevanandam et al. researched Al_2O_3 and MgO nanoparticles for the adsorption of thiophene from hydrocarbons.[31] Nanocrystalline MgO and Al_2O_3 did not show any adsorption capacity. Since thiophene is a soft Lewis base, soft Lewis acid sites are necessary to polarize the thiophene, similar to the acidic zeolites described previously. Al_2O_3 was then impregnated with silver via Agacac, which performed better at removing thiophene than unimpregnated Al_2O_3. The adsorbent adsorbed 0.022 mmol/g of thiophene and 0.009 mmol/g of benzothiophene in isooctane. It did not adsorb dibenzothiophene or 4,6-dimethyl dibenzothiophene. Regeneration for thiophene adsorption was possible in air at 170°C for thiophene and 250°C for 2 hours for benzothiophene.

Ko et al. studied the surface and size influences of Ni nanoparticles on sulfur compound adsorption.[43] Nickel nanoparticles were less than 5 nm in size and supported in the pores of SBA-15. Figure 5 shows that an increasing in Ni loading led to larger the particle sizes and reduce sulfur capacity as shown by figure 5. Ni nanoparticles were also synthesized in a solution with a capping agent. The capping agent was used to maintain the particles' small size, but prevented their complete reduction under H_2. Therefore despite their small size, sulfur capacity decreased.

In 2007, Yang et al. investigated xerogel-derived zinc-based nanocrystalline Al_2O_3 for the adsorption of thiophene from pentane at ambient temperatures and pressures.[44] A thermovacuum treatment at 500°C for 3 hours creates a defected surface spinel structure formed on the nanoparticles' surface. The weak bonding between zinc ions and Al_2O_3 support allowed the zinc to strongly adsorb thiophene from the hydrocarbon solution. The

sorbent could be regenerated to more than 96% of its original capacity via a 1 hour thermovacuum treatment at 500˚C.

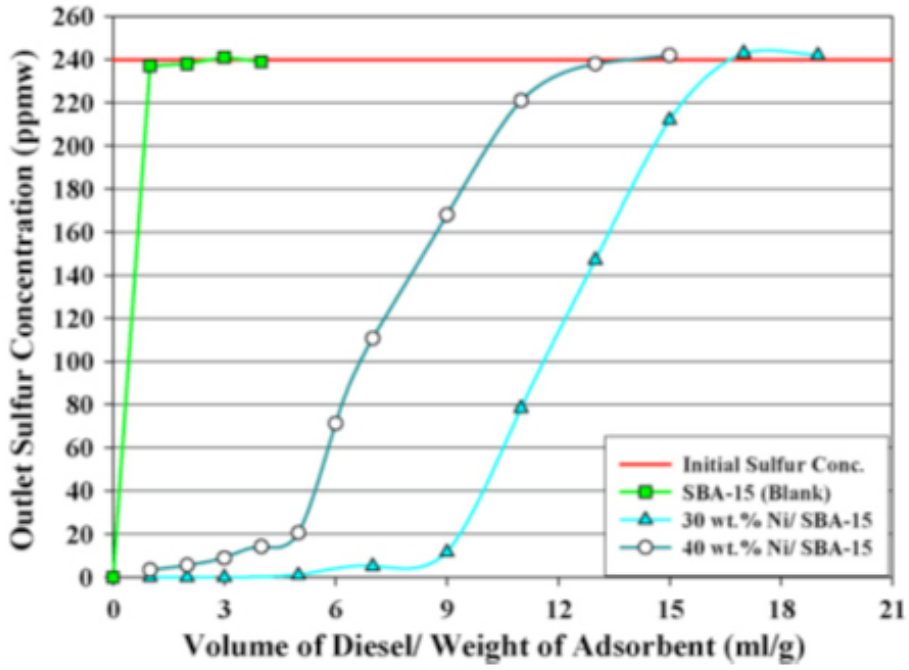

Fig. 5: Breakthrough curves for sulfur compounds in commercial diesel with various types of Ni impregnated adsorbents.[43]

CHAPTER 3

EXPERIMENTAL PROCEDURES

In this chapter, the techniques used to prepare, characterize and test samples are discussed. Combustion chemical vapor condensation was employed to synthesize $NiAl_2O_4$ nanopowder sorbents. The powders were then processed into pellets prior to being placed into the reactor and exposed to model fuels. Characterization was completed using x-ray diffraction (XRD), thermogravametric analysis (TGA), transmission electron microscopy (TEM), surface area analysis, interstitial gas analysis (IGA), and x-ray photoelectron spectroscopy (XPS).

3.1 Nanopowder Synthesis via Combustion Chemical Vapor Condensation (CCVC)

Combustion chemical vapor deposition (CCVD), developed by Hunt et al., is a patented, open-atmosphere, aerosol-based technique for creating thin-films of metals, oxides, and others at a lower cost and faster deposition rate than other vapor-based processes.[45] CCVC is a modified version of CCVD where precursor solution droplets are not deposited on a surface, but instead ignited in air to form solid particles. By adjusting solution chemistry, temperature distribution, and residence time in the flame, a large number of experimental compounds can be synthesized and tested with varying compositions. It has been shown that this process can create single particles less than 20 nm and with specific surface areas between 50 and 200 m^2/g.[46]

The CCVC process shown in figure 6 consists of six steps. First, the precursor organic solution is prepared by mixing metal containing chemicals with appropriate solvents. If

mixed metal oxides are desired, the precursors are mixed in ratios based on the stoichiometry of the desired material. Organic solvents are added to decrease viscosity and allow the solution to be easily atomized. A low-flow pump (Shimadzu LC-6AD) feeds the solution into the Nanomiser^{TM} device, which sprays the solution creating an ultra-fine mist. The mist is then ignited in air or oxygen in a high velocity flame. The solute condenses, dries, and sinters to form dense particles. The Nanomiser^{TM} device allows the use of any soluble precursor without concerns about vapor pressure.

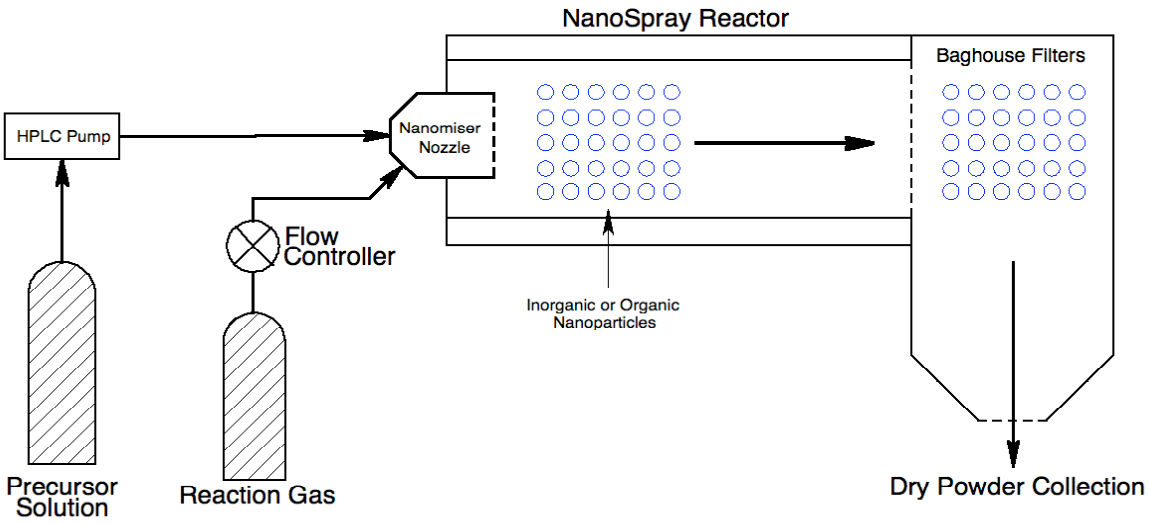

Fig. 6: Schematic for the production of nanoparticles via CCVC.

Given that the precursors are ignited and cooled too quickly for diffusion-controlled growth to take place, the particles remain nanoscale in size. The powder is quenched downstream to inhibit agglomeration, and then collected.

3.2 Raw Materials

Prior to synthesizing and testing $NiAl_2O_4$ for this work, metal oxides supported on yittria-stabilized zirconia (YSZ) were tested. CuO, NiO and ZnO supported on YSZ were synthesized using CCVC, characterized using BET, TEM, and XRD, then reduced under H_2 and tested for sulfur adsorption capacity. With the exception NiO-YSZ, all displayed little to no affinity for sulfur. Nickel metal has been used as a catalyst for the reduction of H_2 gas in fuel cells and is poisoned by H_2S in the gas stream.[47] When placed in a reducing atmosphere at high temperatures, nickel is leeched out of the spinel structure, forming Al_2O_3 supported nickel metal. The nickel can then be used to achieve the deep desulfurization of benzothiophene from dodecane. Furthermore, $NiAl_2O_4$ is less difficult to synthesize via CCVC and precursor solutions are both less expensive and easier to attain than NiO-YSZ.

To synthesize $NiAl_2O_4$ via CCVC, a solution of 13% nickel octoate (Shepard Chemical Co.) and 11% aluminum tri-secondary-butoxide (Chattem Chemicals, Inc.) were mixed in precise stoichiometric ratio. An excess of toluene (Alchemy-South, Ltd.), propane and 2-ethyl hexanoic acid (BASF) were added to the solution to reduce the viscosity and improve the performance of the Nanomizer^{TM} device. Flow rates and other processing conditions are proprietary to nGimat.

Model fuels with a sulfur concentration of 300 ppmw were mixed using dodecane (Acros Organics) and benzothiophene (98+% pure, Alfa Aesar).

3.3 Pellet Preparation

Due to their size, nanopowders flow similar to that of a liquid in the loose aggregate form. When placed inside a reactor vessel under the flow of fuel, the powder can easily become fluidized, and travel outside the reactor into piping, obstructing the flow. This leads to clogging and erroneous measurements. In addition, the packing density of the powder is such that only a few grams of adsorbent can be placed into the reactor for study. Furthermore, it is important to ensure that the fuel is exposed to the entire surface area of the adsorbent. These issues made it difficult to develop repeatable results. As a consequence, the powders were formed into porous pellets. This step allowed for double the amount of adsorbent to be loaded into the reactor, complete wetting of the surface by the fuel, and significantly less clogging. Additionally, the additional adsorbent inside the reactor vessel also allowed the desulfurization of model fuels to be observed more clearly.

To create pellets with a minimal loss in surface area, isopropyl alcohol (Alchemy-South, Ltd.) and an aqueous solution of 2 wt% 2-methoxyethanol (1600 cPs, Alfa Aesar) were mixed with the powder (fig. 7A) in a weight ratio of 4.5:1.6:1, respectively. The slurry was deposited as droplets onto a hot plate at a temperature of 60°C with a pipette and allowed to set for 1 hour. Afterwards, they were fired at 600°C for 6 hours at a ramp rate of 100°C/hr to burn out the binder. The resulting pellets, shown in figure 7B, were loaded into a reactor for fixed-bed adsorption experiments.

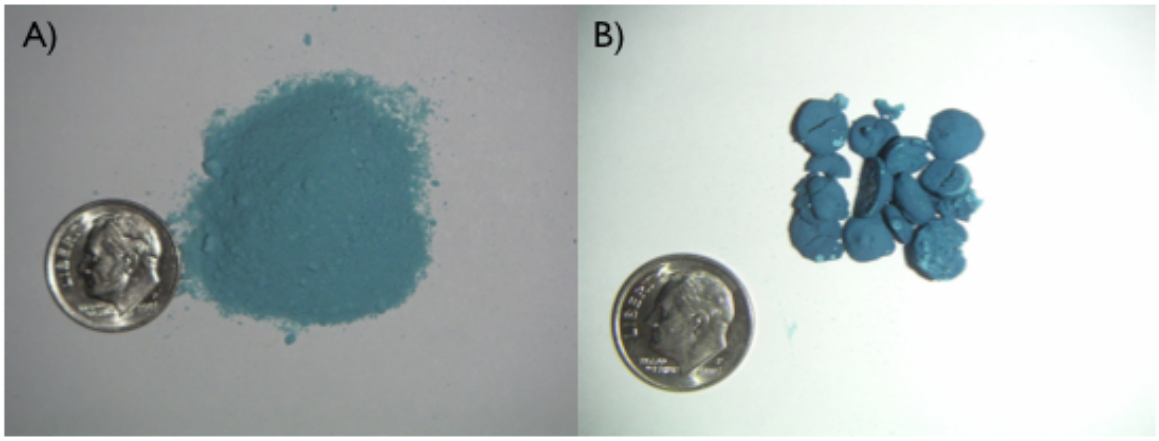

Fig. 7: Optical photographs of $NiAl_2O_4$ nanopowders prior to pellet formation (A); pellets after firing for 6 hours at 600ºC (B).

3.4 Fixed-Bed Adsorption Experiments

Adsorption experiments were carried out using a fixed-bed reactor vessel setup depicted in figure 8. Nanopowder pellets (~10g) were loaded into the reactor between two layers of Kaowool insulation. Once sealed, the reactor was heated to the desired temperature at a rate of 50°C/min. Once the experimental activation temperature was attained, H_2 gas (100% H_2, Airgas) was passed through the reactor at a rate of 250 ml/min for a designated activation time. It was then cooled under H_2 to 150°C. The materials, activation times, temperatures and experimental conditions tested are compiled in Table 4. Model fuel containing 300 ppmw S due to benzothiophene was then passed over the adsorbent at a rate of 2 ml/min. Prior to each experiment, the pump was calibrated to ensure accurate flow rates.

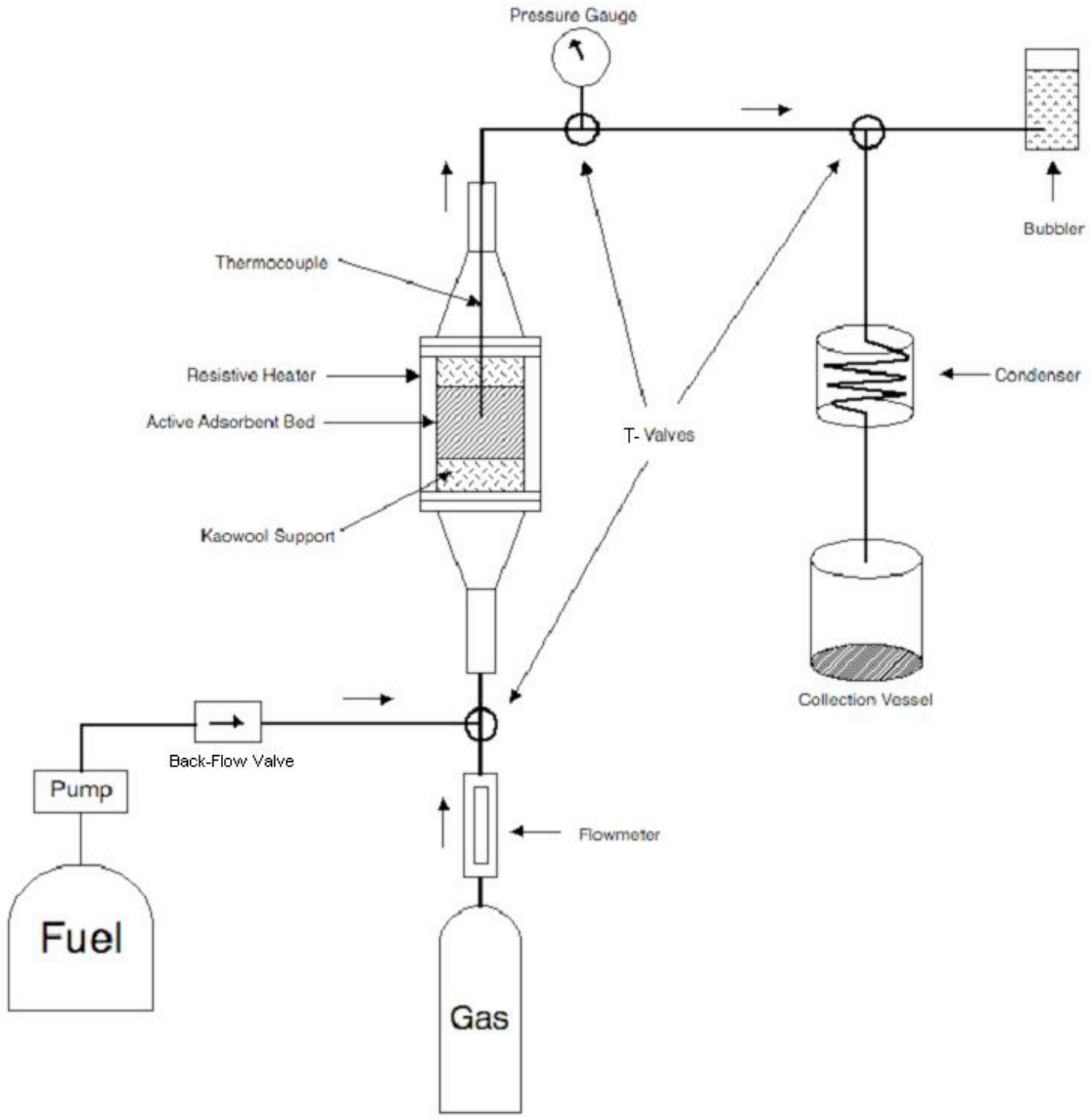

Fig. 8: Schematic of the fixed-bed adsorption reactor system.

Regeneration experiments were completed using $NiAl_2O_4$ after 3 hour reduction at 500°C, and then exposed to model fuel at 150°C until the sulfur concentration in the effluent fuel matched model fuel concentration. Before hydrogen regeneration, the used adsorbent was dried in air at 250°C for 12 hours, then loaded into the reactor and heated to 500°C at a ramp rate of 50°C/min for 2 hours under H_2 with a flow rate of 250 ml/min. Air regeneration was carried out by placing the used adsorbent into a furnace and heated

to 700°C at a ramp rate of 200°C/hr for 1 hour. Afterwards, it was reduced at 500°C for 3 hours before exposure to fuel at 150°C. In all experiments, H_2 was applied during cooling from reduction temperatures.

Table 4. Conditions tested for benzothiophene adsorption.

Activation Temperature (ºC)	Activation Time (hours)	Adsorption Temperature (ºC)
200	3	150
300	3	150
400	3	150
500	3	150
500	3	150
500	1	150
500	2	150
500	3	100
500	3	50
600	3	150

After reduction, fuel flow began and samples of 1 ml each were taken at 2 minute intervals starting from when fuel began flowing at the outlet until sulfur concentrations rose above 100 ppmw S. Subsequent collections were taken at 5 minute intervals. The fuel samples were loaded into a Hewlett Packard 5890 Series II gas chromatograph equipped with a flame photometric detector (GC-FPD) and an autosampler that injected 1 µl of each sample. The GC-FPD heating element was set to an initial temperature of 150˚C and ramped to 220˚C at a rate of 40˚C/min, then to 223˚C at a rate of 1˚C/min during each run. The total run-time was 4.75 min. A second GC-FPD method was used to determine if other thiophenic compounds were present in the effluent fuel. After ramping

to 220˚C, the GC-FPD was heated to 225˚C at a ramp rate of 0.1˚C/min, and the total run time was 51.75 min.

Under these conditions, dodecane spiked with benzothiophene produced peaks at a retention time of 3.99 min, as shown in figure 9. The area of the peak detected in each fuel sample was measured using the Enhanced Chem Station (Hewlett Packard) software package. Fuel samples with known concentrations (0, 10, 27, 79, 287, and 302 ppmw S) were run before each experiment to develop a calibration curve that correlates the area of the benzothiophene peak to sulfur concentration within the fuel. The plateau in counts in the 302 ppmw sulfur peak was attributed to signal saturation of the detector. As a result, the integral of the peak is in error, and instrumental calibration curves omit this point.

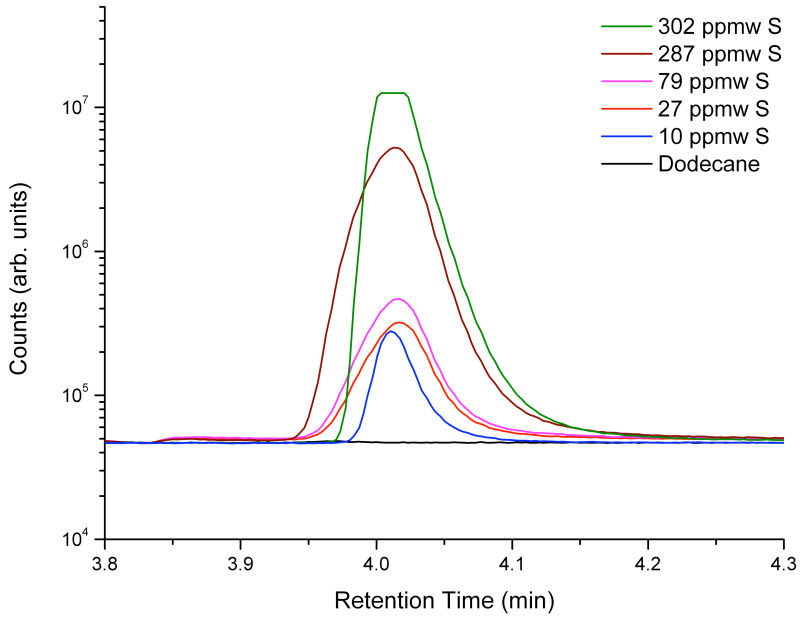

Fig. 9: GC-FPD chromatograms corresponding to 0, 10, 27, 79, 287, and 302 ppmw S samples.

As sulfur concentration in the standard samples increased to more than 100 ppmw sulfur, the instrument response became non-linear. Trace analysis is most important for

desulfurization, therefore only the linear portion of the curve from 0 to 79 ppmw sulfur was fit using the calibration curve. Above 100 ppmw S, a linear fit underestimated sulfur concentration in the samples, and as a result, the adsorption data presented in this research do not show adsorbent saturation.

Each adsorption experiment was run until the sulfur concentration in the effluent matched the concentration of the model fuel. The data in figure 10 were fit with a linear function and a y-intercept of zero. The R^2 value of each fit was no smaller than 0.99, and each calibration sample was tested five times to determine the error associated with each the measurement. The standard deviation of each data point was smaller than the size of the points.

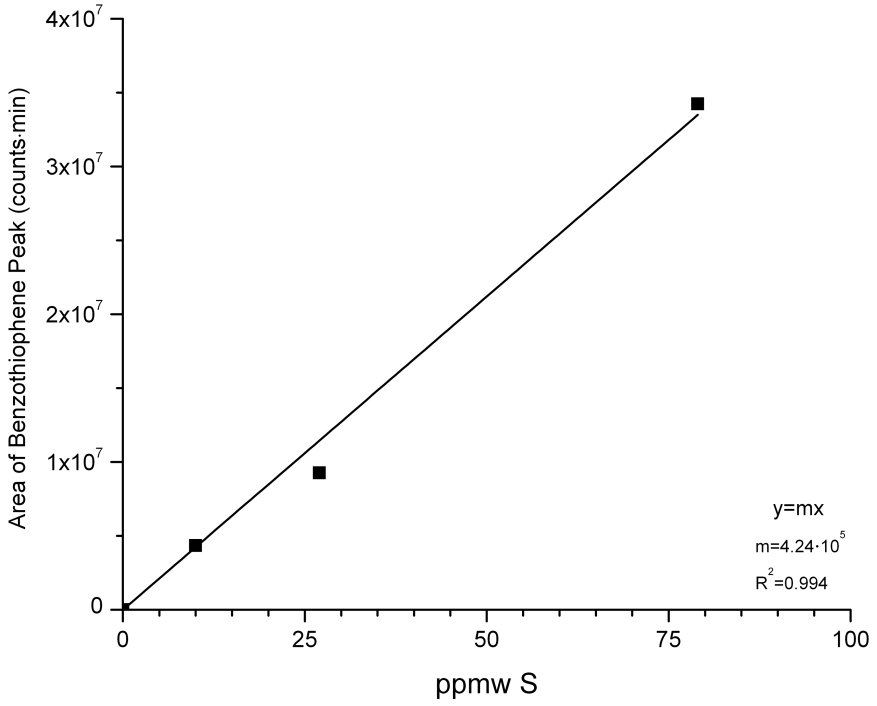

Fig. 10: A typical calibration curve fit by a linear equation.

Based on these calibration curves, the GC-FPD results from individual experimental fuel samples were used to construct breakthrough curves for each adsorbent test. Breakthrough curves, like the one shown in figure 11, were constructed by plotting the measured sulfur concentration of the effluent fuel versus the volume of fuel passed per gram of adsorbent material. The breakthrough capacity is defined as the volume of fuel cleaned to below 15 ppmw sulfur, which is the maximum sulfur concentration allowed to adhere to EPA emissions standards and prevent significant fouling of catalytic converters.

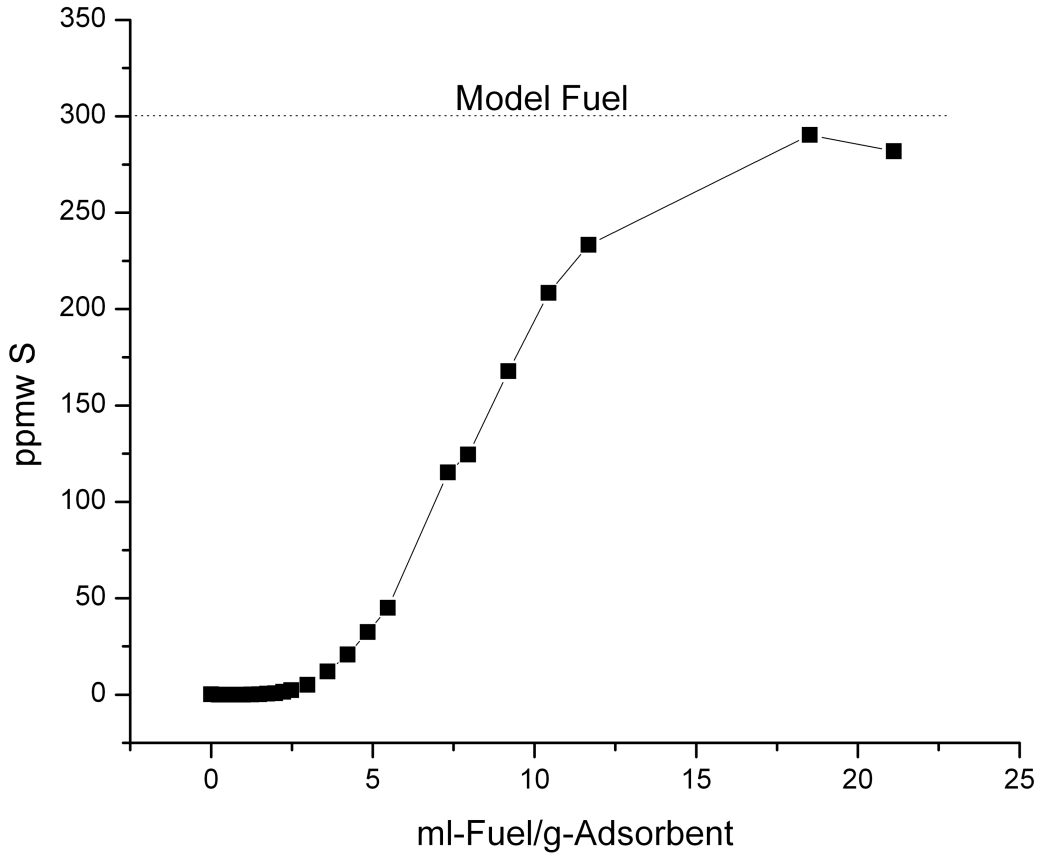

Fig. 11: Breakthrough curve constructed using the GC-FPD data from each fuel sample collected.

Molar adsorption amounts (normalized per adsorbent weight) were obtained by solving the following equation:[48]

$$q_{breakthrough} = \left(\frac{v \rho_{fuel} X_i}{m_{adsorbent} MW_{sulfur}} \right) \int_0^t \left(1 - \frac{C(t)}{C_i} \right) dt \qquad (1)$$

where $q_{\text{breakthrough}}$ is the total sulfur adsorbed at breakthrough (mol/g), v the flow rate of fuel (cm^3/min), ρ_{fuel} is the density of dodecane at room temperature (g/cm^3), X_i is the total sulfur fraction by weight in the model fuel, $m_{\text{adsorbent}}$ the weight of the adsorbent bed (g), MW_{sulfur} the molecular weight of sulfur, C_i the total sulfur concentration in the model fuel (ppmw S), and $C(t)$ is the effluent sulfur concentration (ppmw S) at time, t (min).

Possible sources of error involved in these measurements should be noted. First, fuel flow was not always constant at the outlet. After an experiment was completed, the volume of fuel passed was measured and averaged over the total collection time to determine an average flow rate. The inconsistency in fuel flow leads to an uncertainty in the abscissa estimated to be ±0.2 ml of fuel per gram of adsorbent. Furthermore, the response of the GC-FPD did not completely conform to the calibration curve developed. Based on the calculated R^2 value, an error of 6% is introduced in to the sulfur concentration measured. Each experiment conducted was repeated to confirm the results.

3.5 Characterization

Several characterization methods were used to identify the phases present, measure physical properties, and observe the particles created by CCVC. These techniques include: x-ray diffraction (XRD), x-ray photoelectron spectroscopy (XPS),

thermogravimetric analysis (TGA), transmission electron spectroscopy (TEM), surface area analysis, and interstitial gas analysis (IGA).

3.5.1 X-Ray Diffraction

XRD analysis was performed using a PANalytical X'Pert Pro Diffractometer and Cu K_α radiation (λ=1.54Å) with a working voltage and current of 45 kV and 40 mA. Powder samples were mechanically pressed to improve the signal-to-noise ratio. Continuous measurements between 25º and 100º 2θ were attained using a scan rate of 0.094º/min at 0.033º increments. Intensities were normalized to the 440 peak in $NiAl_2O_4$, and phase identification was carried out using the Jade 7 software package (Materials Data, Inc.).

Williamson-Hall particle size analysis was used to calculate crystallite size.[49] This technique correlates the broadening of XRD peaks to the size of the particles present in the sample. The full-width-at-half-maximum, B, of the (400), (440), and (444) peaks were measured and plotted on a scale of $B\cos\theta/\lambda$ versus $\sin\theta/\lambda$, where θ is the angle at which the peak occurred and λ is the x-ray wavelength. Linear regression analysis was used to determine the y-intercept, which was inserted into equation 1 to determine crystallite size, t.

$$y - \text{int} = \frac{B\cos\theta}{\lambda} = \frac{0.9}{t} \qquad (2)$$

3.5.2 X-Ray Photoelectron Spectroscopy

XPS analysis was performed in an ESCA-SSX 100 instrument using monochromatized Al K_α radiation with photon energy of 1486.6 eV. The operating pressure was 10^{-8} Torr

or less. The binding energy scale was calibrated using the 2s line of Al^{3+}, centered at 117.6 eV. Measurements of $NiAl_2O_4$ required the use of a low-energy electron flood gun to neutralize charging during analysis. Before measurements were made, it was confirmed that the powders did not obviously differentially charge by collecting spectra at several flood gun settings and confirming no changes in peak shape.

General surveys of the sample surfaces were measured using 15 scans within a range of 0 to 1100 eV at 1 eV increments using an x-ray spot size of 800 μm and a pass energy of 150 eV. To determine surface composition, 5 samples of each material were tested, and the average composition is reported.

High energy resolution scans of Ni 2p peaks were conducted with 1,500 scans at 0.1 eV increments using an x-ray spot size of 400 μm and a pass energy of 50 eV. Peak fitting used symmetric curves that were 80% Gaussian and 20% Lorentzian. Analysis of the measurements was carried out using the ESCA 2005G software package provided by Service Physics, Inc.

3.5.3 Transmission Electron Microscopy

TEM studies were used to characterize the particle size and obtained on a Hitachi H-800 electron microscope operated at 100 kV at nGimat Inc.

3.5.4 Thermogravimetric Analysis

TGA was performed using a TA Instruments Q500 at nGimat Inc. Samples were placed into an alumina sample cup and heated to 800ºC at a rate of 5ºC/min. Samples were then allowed to cool to 190ºC. H_2 or air atmospheres were used with a balance purge flow rate of 40 ml/min and a sample purge flow rate of 60 ml/min.

3.5.5 Surface Area Analysis

Specific surface areas (SSA) were estimated by the BET (N_2) method in a Quantachrome Quantasorb sorptometer at nGimat Inc. Samples (~50 mg) were degassed at 250ºC for 3 hours. Analysis was conducted at -196ºC with N_2 as the adsorbate gas. The SSA's were then calculated using the BET multipoint method. Average particle size as derived using the following equation:[50]

$$r = \frac{3}{\rho \cdot SSA} \qquad (2)$$

Where ρ is the theoretical density of the material and r is the particle radius.

3.5.6 Scanning Electron Microscopy

Pellet morphology was examined using a Leo 1530 SEM equipped with a secondary electron detector at pressures below 10^{-6} Torr. The SEM was outfitted with an energy dispersive spectroscopic (EDS) analyzer (Oxford Instruments) and INCA analysis software. EDS allows for the detection of elements and their relative abundance. However, the information gathered through this technique can only be interpreted

qualitatively. EDS was used to determine if sulfur is present on the surface of $NiAl_2O_4$ after fixed-bed adsorption experiments.

3.5.7 Interstitial Gas Analysis

The amount of sulfur adsorbed to $NiAl_2O_4$ was measured using IGA. The Evans Analytical Group (Syracuse, NY) conducted tests and analyzed the samples submitted. The technique was specifically sensitive to sulfur and error is estimated to be 15%.

CHAPTER 4

RESULTS AND DISCUSSION

In this section, results of characterization and fixed-bed adsorption experiments on $NiAl_2O_4$ are discussed. Based on observations and data collection, reasons for capacity and mechanisms for deactivation are proposed. Various H_2 reduction and reactor conditions are tested to determine the optimum conditions for desulfurization of model fuel.

4.1 Nanopowder Adsorbent Characterization

XRD data, shown in figure 12, confirmed that the material was crystalline $NiAl_2O_4$ spinel (PDF 01-073-0239).[51] Peaks were indexed according to the PDF file from the International Center for Diffraction Data (ICDD) database. The intensity of the peaks did not entirely agree with the PDF, but this is likely due to the introduction of a preferred orientation due to mechanical pressing of the sample prior to analysis.

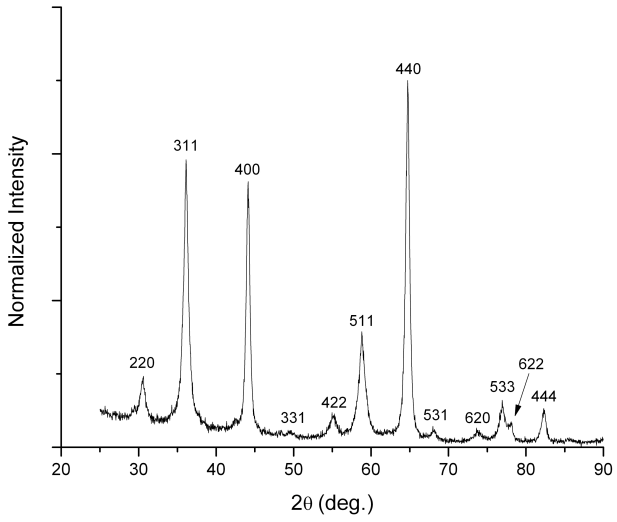

Fig 12: XRD analysis of the powder synthesized via CCVC corresponds to cubic spinel $NiAl_2O_4$ (PDF 01-073-0239).

Han et al. noted that the synthesis of $NiAl_2O_4$ is sensitive to stoichiometry.[52] Any excess nickel or aluminum that cannot react stoichiometrically during synthesis causes the formation of that particular oxide along with $NiAl_2O_4$. EDS detected only nickel, aluminum, and oxygen within the material. Therefore the powders did not become appreciably contaminated during synthesis. However, EDS cannot accurately determine atomic concentration to the precision necessary to rule out minor deviations from stoichiometry. However, NiO nor Al_2O_3 phases were detected by XRD, therefore excess oxides did not appear to be a significant issue.

A Williamson-Hall XRD line-broadening plot, shown in figure 13, determined the average particle size to be 12.7 nm. Linear regression of the points produced the equation listed in figure 13 with an R^2 value of 0.986. Error was determined to be less than the size of the data points.

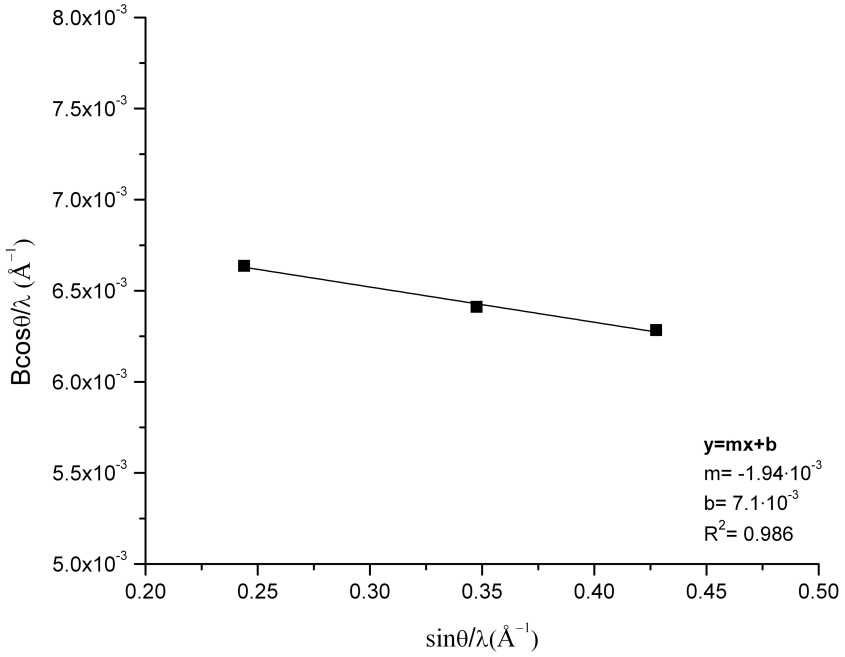

Fig 13: Williamson-Hall plot of the (400), (440) and (444) diffraction peaks.

The results of surface area analysis on $NiAl_2O_4$ powders and pellets are in Table 5. The powder had a specific surface area of 57.8 m^2/g. Using the theoretical density of 4.51 g/cm^3 reported in the ICDD PDF file and equation 2, the average particle size was calculated as 11.5 nm. This is in good agreement with the XRD analysis.

A modest increase in specific surface area to 63.4 m^2/g was observed after the powders were formed and fired into pellets. The similar surface areas between powders and pellets suggest that sintering was not a significant issue despite the large driving force due to the small size of the $NiAl_2O_4$ crystals.

Table 5. BET specific surface areas and average particle size measurements.

Material	Powder Surface Area (m^2/g)	Pellet Surface Area (m^2/g)	Average Particle Size XRD (nm)	Average Particle Size BET (nm)
$NiAl_2O_4$	57.82	63.42	12.7	11.5

SEM images of the pellets after firing are shown in figure 14 and some large particle agglomerates of about 10 μm are present. However, most agglomerates appear to be 1-3 μm across or less. The dark spots in the image are small pores of about 1 μm in diameter that allow the fuel to wet the entire pellet inside the reactor.

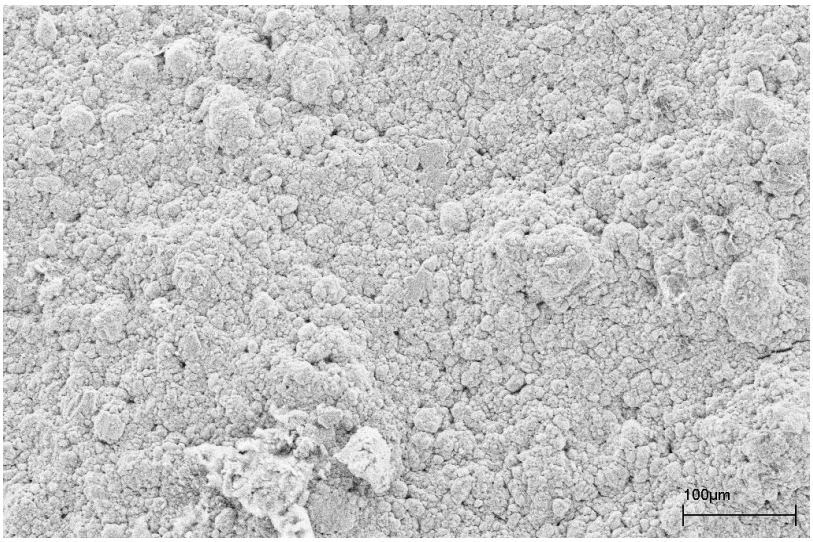

Fig 14: SEM image of $NiAl_2O_4$ nanopowders after firing to form pellets (150X).

TEM images captured the size of the general particle population as well (fig. 15). The particles tended to be spherical and less than 80 nm in diameter, with the majority being less than 40 nm. These images further corroborate the BET and XRD data and show that high surface area nanopowders of $NiAl_2O_4$ are indeed synthesized via CCVC.

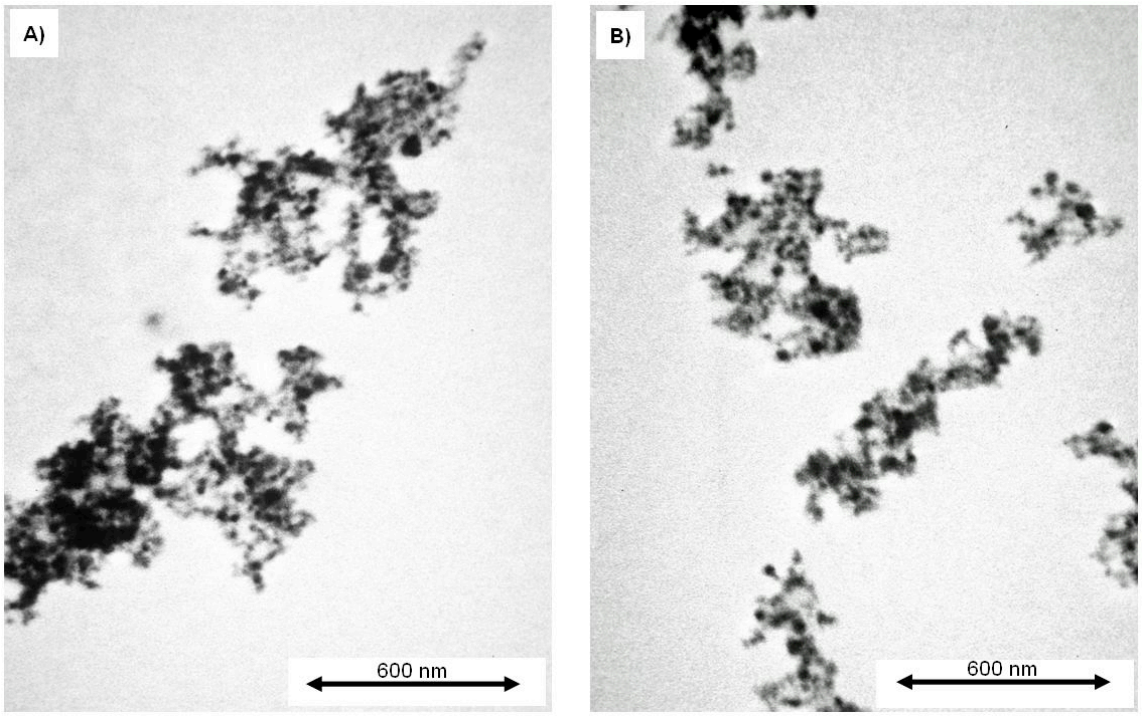

Fig 15: TEM images of the $NiAl_2O_4$ nanopowders (A and B) synthesized at nGimat Inc.

4.2 Initial Adsorbent Studies

At the beginning of this project, adsorption experiments were completed using nanopowders of yittria-stabilized zirconia (YSZ) supported transition metal oxides: CuO, ZnO, and NiO. As described previously, when copper, nickel, or zinc are reduced in zeolite matrices or in nanocrystalline forms, these ions have shown affinity for thiophenic compounds in fuels.[9] The adsorbents synthesized were a 50-50 mix of YSZ and metal oxide catalyst. After a 3 hour H_2 reduction at 500ºC, with the exception of NiO-YSZ, all showed zero sulfur adsorption capacity when exposed to the model fuel.

The success of NiO-YSZ led to the examination of $NiAl_2O_4$, reduced under hydrogen flow. XRD analysis after the reduction step (fig. 16) shows that $NiAl_2O_4$ is reduced, forming nickel supported on σ-Al_2O_3 and $NiAl_2O_4$. Unreduced $NiAl_2O_4$ showed no detectable NiO in the material due to excess nickel precursors during production. Therefore it is believed that the presence of nickel metal is due to a chemical reduction of $NiAl_2O_4$ in contact with the H_2 gas.

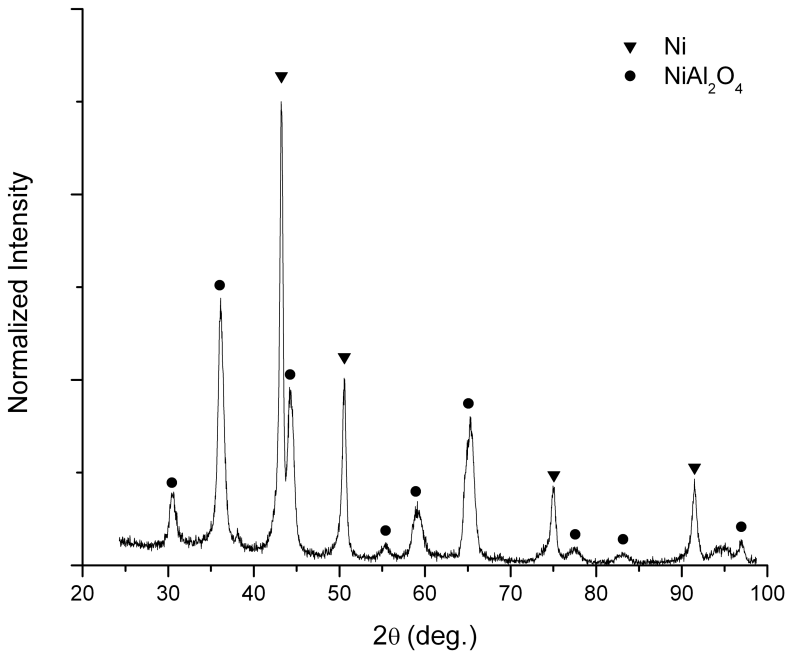

Fig. 16: XRD analysis of $NiAl_2O_4$ pellets after H_2 reduction and subsequent adsorption experiment.

The reduced $NiAl_2O_4$ was exposed to a model fuel flow at 150˚C, and the results of fixed bed adsorption are presented in figure 17. $NiAl_2O_4$ cleaned 2.1 ml-fuel per g-adsorbent to less than 1 ppmw sulfur and 3.4 ml-fuel per g-adsorbent to less than 15 ppmw sulfur. As more model fuel was passed through the reactor, the sulfur concentration of the effluent increased dramatically as reactive sites reached saturation. If a complete removal of benzothiophene is assumed until 1 ppmw S, 14.5 μmol-S per g-adsorbent was captured by the adsorbent material. These values are similar to other nanocrystalline adsorbents described previously.[42] When unreduced $NiAl_2O_4$ was tested, no adsorption capacity was observed, therefore it is believed that deep desulfurization is achieved as a result of the nickel present on the $NiAl_2O_4$ surface. It would also follow that capacity will increase as more reduced nickel is available within the material.

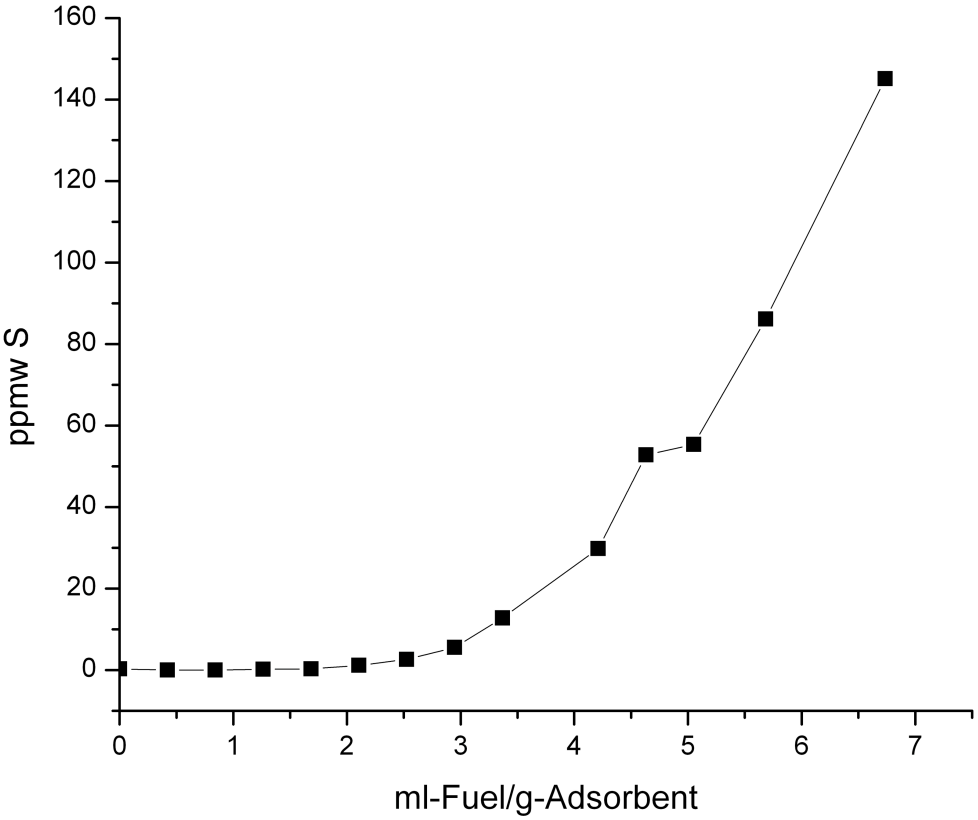

Fig. 17: After a 3 hour reduction in H_2 flow at 500˚C, $NiAl_2O_4$ was able to clean 3.4 ml-fuel per g-adsorbent to less than 15 ppmw S.

In plotting a breakthrough curve, only the peak due to benzothiophene (BT) is examined, however it is possible that benzothiophene was broken into other, smaller sulfur compounds. The FPD specifically detects sulfur compounds injected into the GC. Therefore a more thorough examination of the fuel in the GC-FPD would show if indeed benzothiophene is fragmented into other sulfur species (fig. 18). The extended test showed dibenzothiophene (DBT) is present in the model fuel due to impurities in the source, and both compounds are completely removed by the adsorbent. More importantly, it showed no other S peaks present within the effluent fuel after fixed-bed adsorption.

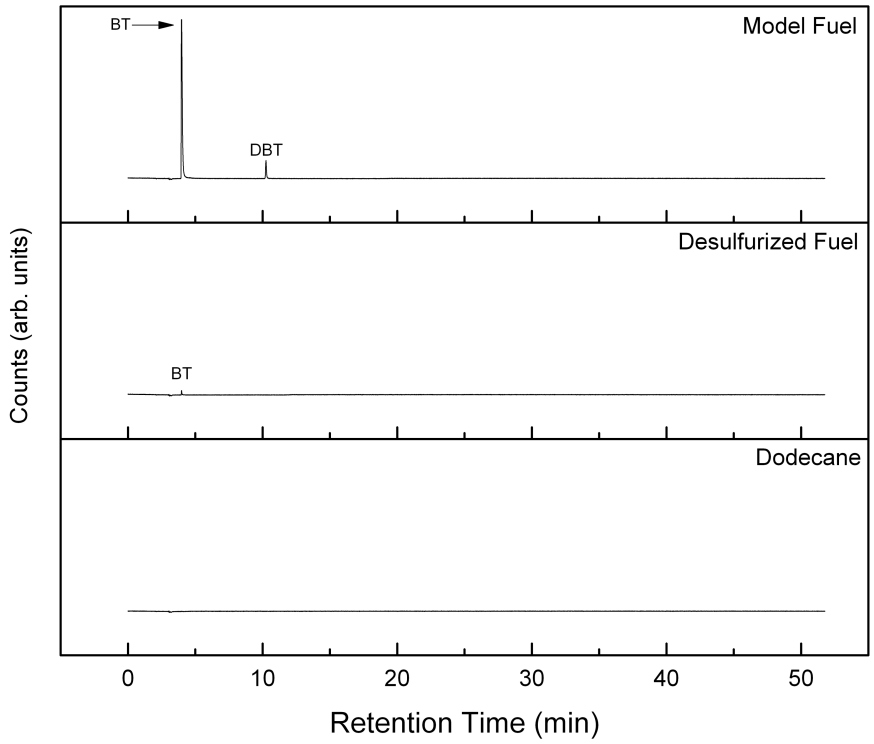

Fig. 18: A GC-FPD test of the desulfurized fuel shows no other sulfur compounds present.

The presence of sulfur on the adsorbent surface would confirm that reduced $NiAl_2O_4$ is sequestering benzothiophene when exposed to the model fuel. However, a high energy-resolution XPS measurement of the S 2p photoelectron line at 166 eV did not detect sulfur in the used adsorbent. The limit for sulfur detection is approximately 1 at%.

Based on the amount of moles of sulfur removed and the moles of $NiAl_2O_4$ present in the reactor, the atomic percentage of sulfur that should be present in the adsorbent can be calculated. The amount of adsorbent in the reactor is known; therefore the molar ratio between sulfur and $NiAl_2O_4$ can be calculated to determine an expected atomic

percentage. With 10.5 g of adsorbent, there would be 0.03 at% S on the sample. This is far too low to be detectable using XPS, which explains the negative result.

IGA analysis of used and unused $NiAl_2O_4$ caused the sulfur present in the material to oxidize and become detectable in small concentrations using infrared detectors. Figure 19 shows the sulfur detected in both samples and the peak areas were compared to standards to measure sulfur concentration. Sulfur content increased from 220 ppmw to 650 ppmw between the unused and used $NiAl_2O_4$. The result confirmed that sulfur is captured by the adsorbent in fixed-bed adsorption experiments. The broad, doublet peak suggests that sulfur is bonded to the adsorbent in multiple ways.

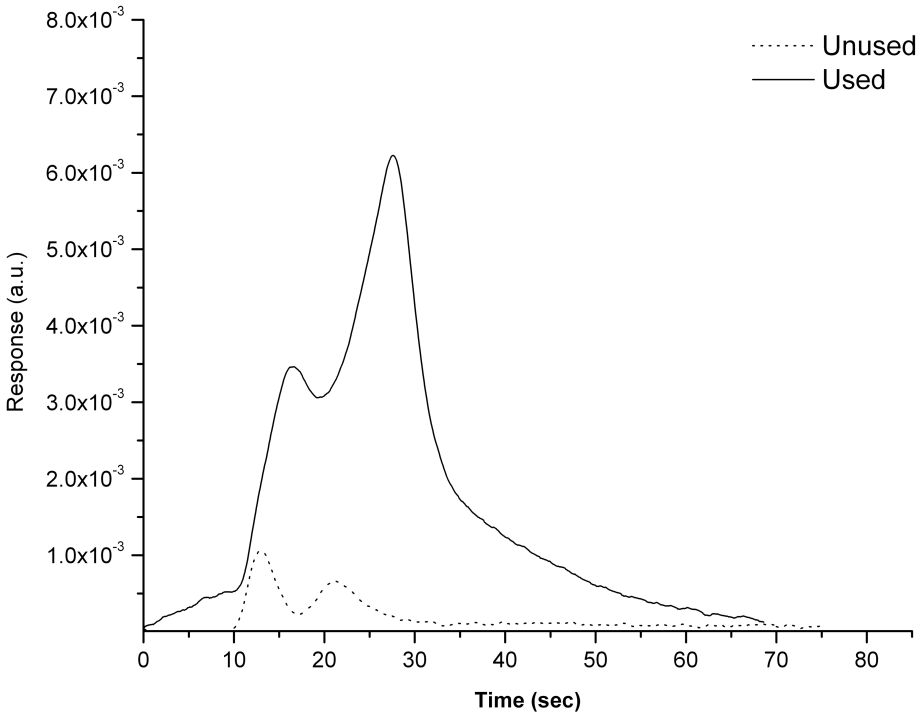

Fig. 19: IGA of unused and used $NiAl_2O_4$.

XPS of the Ni $2p_{3/2}$ peaks from unused and used $NiAl_2O_4$ is shown in figure 20. The measured binding energies of elements in both samples are listed in table 6. The results indicated two forms of nickel in the used sample due to two observed peaks at 853.7 eV and 850.4 eV. The larger binding energy peak is consistent with NiO and appears in both then used and unused adsorbent.[54] The area of the oxide peak is significant even after reduction, meaning that a majority of the nickel on the surface remains as an oxide.

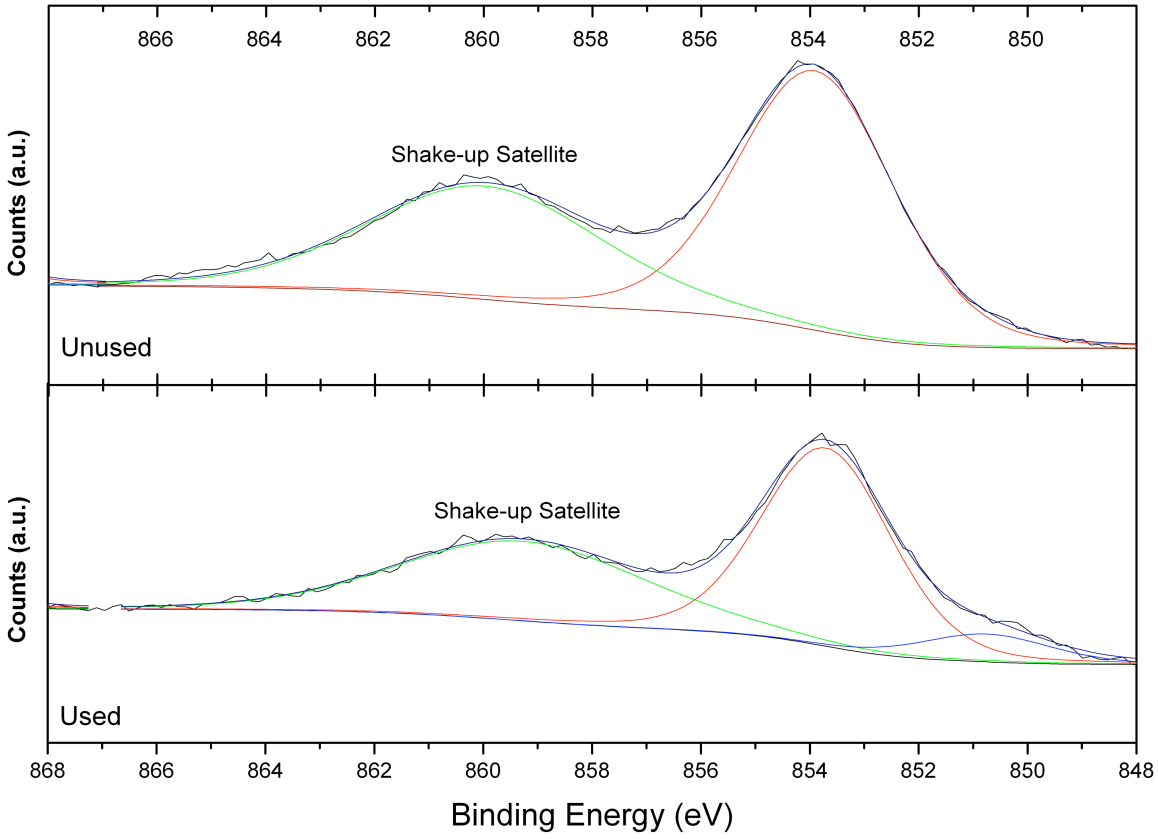

Fig. 20: The XPS spectra of Ni $2p_{3/2}$ peaks in unused and used $NiAl_2O_4$ show a secondary peak at 850.4 eV in the used adsorbent, due to the presence of Ni metal.

Table 6. XPS binding energies of unused and used $NiAl_2O_4$.

Material	Binding Energies (eV)					
	Ni $2p_{3/2}$	**Ni $2p_{1/2}$**	**Ni 3p**	**O 1s**	**Al 2p**	**Al 2s**
Unused $NiAl_2O_4$	853.9	871.1	67.0	529.5	72.6	117.6
Used $NiAl_2O_4$	850.8 853.7	871.0 872.0	66.4	529.6	71.7	117.6

The fits of the data had χ^2 values less than 3.0. Binding energies reported in literature for nickel metal and NiS are 852.2 eV and 852.8 eV, respectively, calibrated against adventitious carbon.[55,56] Neither of these reported binding energies are close to the 850.4 eV binding energy measured. However, based on the lack of detectable sulfur and XRD data previously presented, the 850.4 eV peak in the used sample is likely due to nickel. The depth of sensitivity with XPS is 5-10 nm, and the results indicate a large fraction of surface nickel is oxidized, and not taking part in benzothiophene adsorption.

When the adsorbent is removed from the reactor, after adsorption, it appeared black, as shown in figure 21. This observation was characteristic of materials successfully capturing sulfur. BET surface area analysis of the used adsorbent showed a decrease in specific surface area from 63.4 m^2/g to 40.3 m^2/g. Reasons for the loss in surface area will be discussed later and is important when considering the overall desirability of $NiAl_2O_4$ as a regenerable and cyclable adsorbent.

Fig. 21: $NiAl_2O_4$, originally light blue, turned black after reduction and adsorption.

It was hypothesized that the black color of used adsorbent is due to coking of the catalyst. Coke is a carbonaceous agent that is a product of reacting species and deposited on the surface of the catalyst. XPS analysis confirmed an increase in surface carbon concentration. In this case, the carbonaceous material is likely due to the aliphatic hydrocarbon that results after benzothiophene is desulfurized. The carbonaceous material may also clog porosity, thereby reducing surface area.

Figure 22 shows the results of general XPS surveys of both used and unused adsorbent surfaces. The C 1s peak is more pronounced in the used adsorbent, while its nickel peaks are more depressed. The results of surface composition analysis are complied into table 7 and show a 76.9% increase in carbon on the used adsorbent, and a 62% decrease in nickel on the surface. Aluminum and oxygen content remained similar because no reactions are

taking place on these sites. As benzothiophene is removed from the fuel, carbon quickly accumulates, deactivating the catalyst by physically preventing benzothiophene adsorption and reaction. As a result, the carbon layer on the nickel surface must be removed to maximize regenerability.

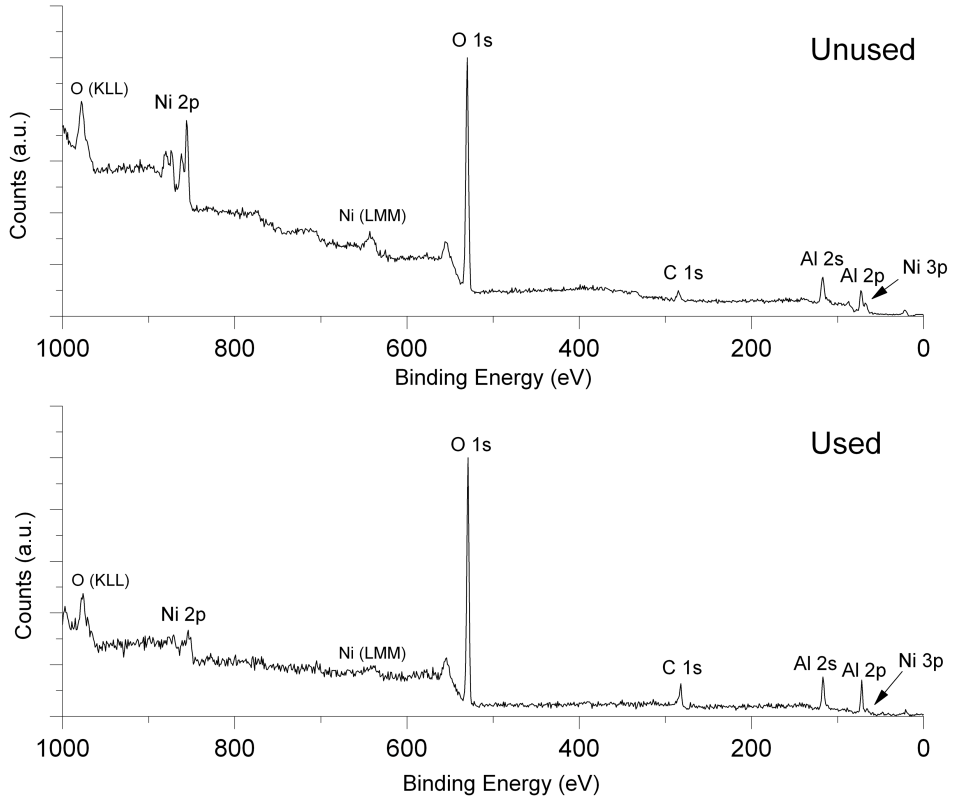

Fig. 22: General XPS surveys of the used and unused sorbents reveal an increase in carbon on the surface.

Table 7. Surface composition measured by XPS.

Material	Composition (at %)			
	Ni 2p	**C 1s**	**Al 2s**	**O 1s**
Unused $NiAl_2O_4$	10	13	21	56
Reduced $NiAl_2O_4$	11	1.9	26	61
Used $NiAl_2O_4$	3.8	23	24	49

4.3 Regeneration of $NiAl_2O_4$ Adsorbents

Once the $NiAl_2O_4$ adsorbent was completely saturated, it was regenerated either by further hydrogen flow at 500˚C for 2 hours or a 1 hour 700˚C treatment in air followed by 500˚C reduction for 3 hours in hydrogen. After the regeneration cycle, the adsorbent cooled under H_2 flow and exposed to model fuel again at 150˚C.

4.3.1 H_2 Regeneration of $NiAl_2O_4$

High-temperature hydrogen regeneration was expected to have two effects: the thermal desorption of benzothiophene from the surface and the creation of more nickel sites through reduction to replace those lost in the previous cycle. Regeneration using H_2 flow also has the advantage of being a single-step process.

The results of the H_2 regeneration step revealed that further attempted reduction led to little recovered capacity (fig. 23). The regenerated adsorbent cleaned 0.9 ml-fuel per g-adsorbent to less than 15 ppmw S and 0.6 ml of fuel per gram of adsorbent to less than 1 ppmw S. This corresponds to 6 μmol and 3.5 μmol of sulfur per gram of adsorbent, respectively. The reason for the small regenerated capacity is believed to be caused by a layer of carbon that forms on the surface of the material during fixed-bed adsorption.

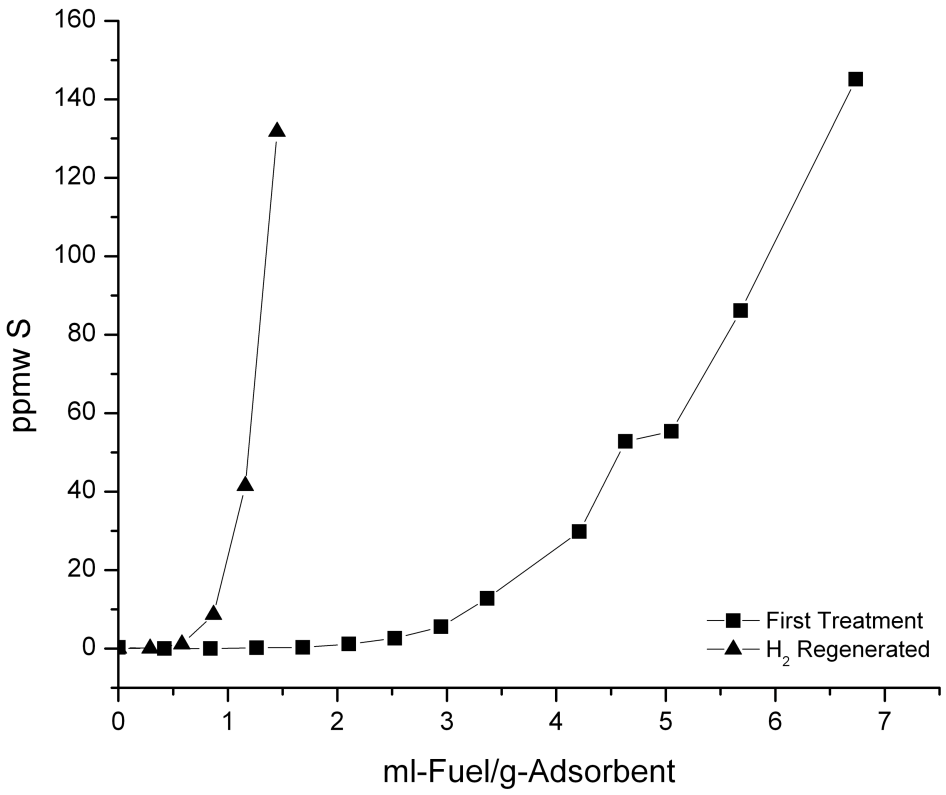

Fig. 23: Breakthrough curves showing the effects of H_2 regeneration.

This carbonaceous layer prevents H_2 gas from reducing more of the $NiAl_2O_4$ to nickel. As a result, nickel sites are not created to replace those that are already occupied by sulfur from the previous test. As more fuel is treated, the amount of carbon deposited onto the surface increases and further cycling was expected to show even less capacity.

Any practical application of a sulfur adsorbent material requires a regeneration process whereby most of the original capacity can be restored repeatedly. Further H_2 reduction did not meet this regeneration requirement as the adsorbent only recovered 25% of its original capcity. Therefore, an alternative approach where carbonaceous material on the surface is burned off in air was investigated.

4.3.2 Air Regeneration of $NiAl_2O_4$

The results of H_2 regeneration revealed that regeneration of spent adsorbent will require the removal of carbon built up on the surface. Heat treatment in air at 700˚C for 1 hour was performed to burn off the surface carbon of used adsorbent. After the regeneration step, the $NiAl_2O_4$ regained its light blue color as shown in figure 24. With the carbon layer removed, H_2 was able to reduce NiO to Ni metal once again.

Fig. 24: Optical photograph of the $NiAl_2O_4$ after the air regeneration step, showing that carbon was removed by the treatment.

XRD on the heat-treated samples showed that during the regeneration step, in addition to carbon burn off, the reduced nickel was oxidized to NiO (fig. 25). From the XRD, it appears that active nickel may have been lost or not oxidized during the regeneration process because the intensity of the NiO peaks relative to $NiAl_2O_4$ is significantly diminished when comparing the strongest nickel peak to $NiAl_2O_4$ in the reduced sample. There are no other identifiable nickel phases within the XRD pattern.

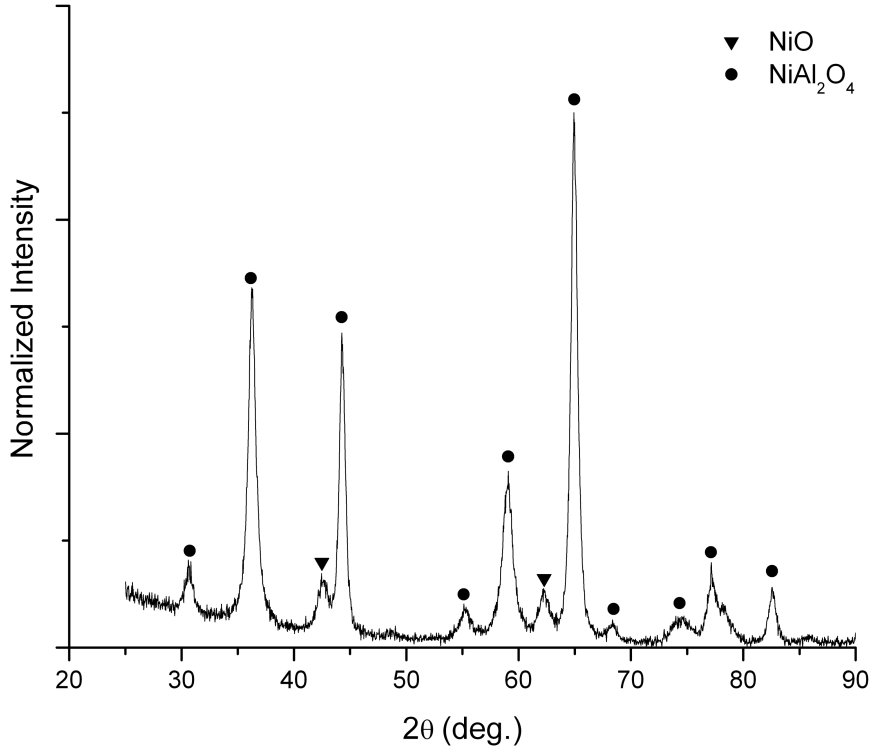

Fig. 25: XRD analysis of the adsorbent after regeneration in air shows the presence of NiO.

To investigate further, XPS was conducted on air regenerated $NiAl_2O_4$. XPS compositional analysis of the air regenerated adsorbent demonstrates that no measurable loss of surface nickel occurred (fig. 26). Peak area measurements show 9.3 at% Ni, which is similar to unused $NiAl_2O_4$ (10 at% Ni). Also, carbon that clogged porosity and decreased surface area is removed by the air regeneration step. Carbon within the adsorbent decreased from 23 at% to 6.3 at%. More significant is the detection of sulfur on the surface of the air regenerated sample, previously undetected in other samples. This finding suggests that during the regeneration process, carbon is reoxidized and removed,

but sulfur is left behind attached, presumably bound to nickel, preventing its oxidation and reduction during the subsequent H_2 treatment.

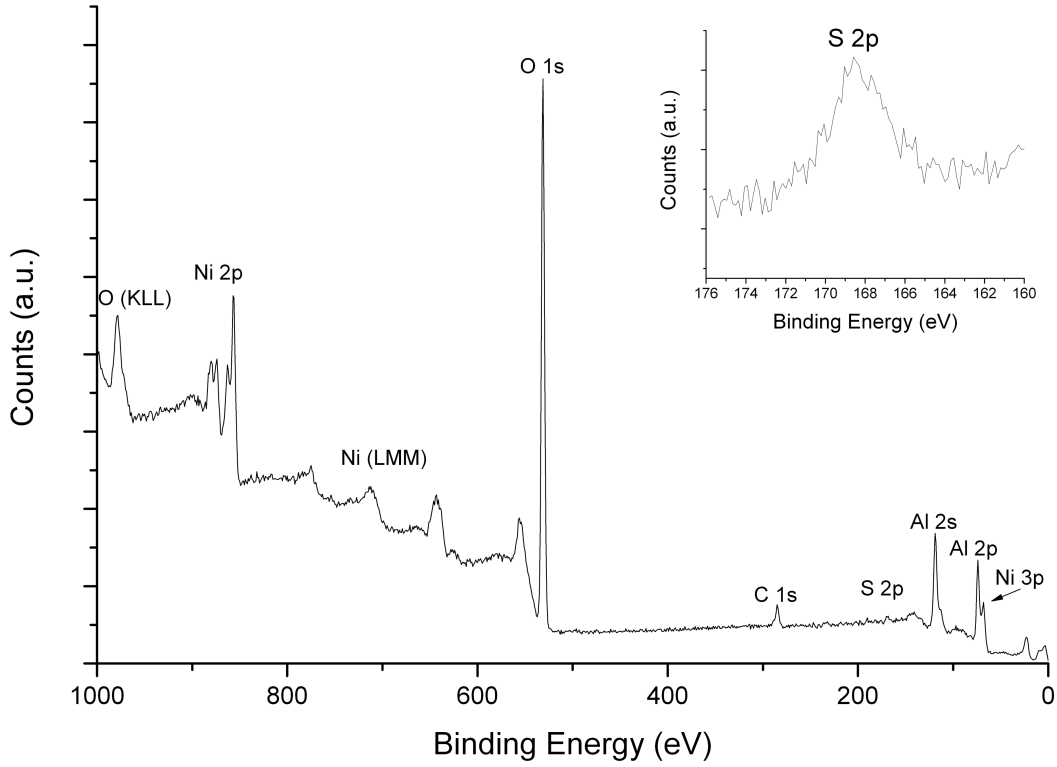

Fig. 26: General XPS survey of air regenerated $NiAl_2O_4$ showing the presence of sulfur (inset).

Furthermore, the surface area of the pellets after air regeneration was 72.7 m^2/g. When compared to the initial measured specific surface area of 63.4 m^2/g, sintering effects can be ruled out. Furthermore, when compared to the used adsorbent surface area of 40.3 m^2/g, it is apparent that surface area was recovered after carbon burn out.

The results of fixed-bed adsorption support again show a significant drop in desulfurization capacity after the first cycle. The air-H_2 regenerated $NiAl_2O_4$ removed benzothiophene from 1.4 ml of fuel to less than 15 ppmw S per gram of adsorbent and 0.35 ml to less than 1 ppmw S (fig. 27). The result is a marginal improvement over H_2 regeneration without carbon oxidation, but it still lost 60% of its original desulfurization capacity. The reason for the considerable decrease in performance cannot be due to a carbonaceous layer preventing nickel reduction because the carbon was clearly removed. Therefore, there must be loss in the amount of active and reducible nickel in the material after the first use.

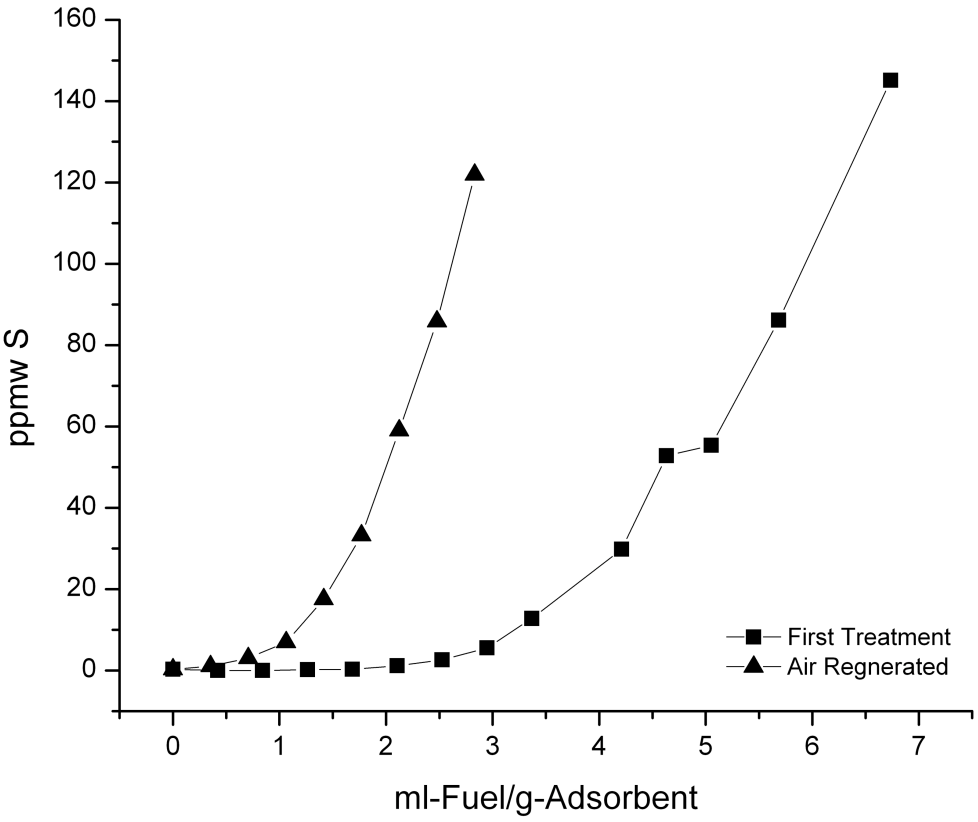

Fig. 27: The results of regeneration show diminished capacity overall, but improved capacity over H_2 regeneration.

High energy-resolution XPS of the Ni $2p_{3/2}$ peaks in air regenerated samples was compared to unused $NiAl_2O_4$ (fig. 28). The results show that the air regenerated adsorbent has two forms of nickel present on the surface (853.9 eV and 852.8 eV) when the peak is deconvoluted by symmetric curves of equal width. The larger binding energy peak is consistent with nickel bound as an oxide.[54] The second peak in the air regenerated sample is centered at 852.8 eV – in between values attributed to NiO and nickel metal. As previously cited, NiS has been observed to occur at 852.8 eV, therefore the second peak is attributed to NiS formed during the high temperature air regeneration step.

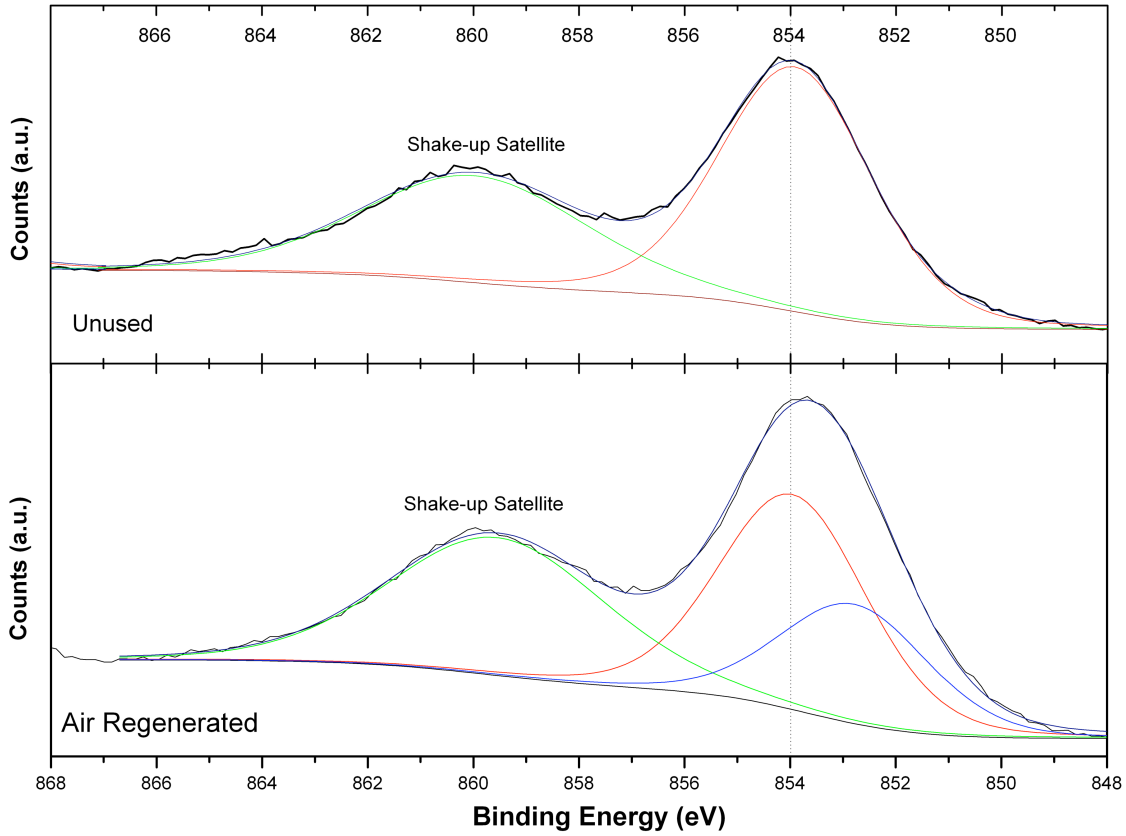

Fig. 28: XPS of the Ni $2p_{3/2}$ peaks from unused and air regenerated $NiAl_2O_4$.

Previous IGA analysis suggested that sulfur is adsorbed to the material in various forms. The samples tested by IGA were used, then heated in air following the previously describe air regeneration procedure. They were not reduced or exposed to model fuel a second time. A sulfur content of 2,900 ppmw was measured within air regenerated samples which is a significant increase over both the unused (220 ppmw S) and used (650 ppmw S) samples (fig. 29). Notice that the IGA measured one strong peak, indicating that sulfur is bound in a single state unlike the sulfur in the used adsorbent. The disparity in measured sulfur content between the used and air regenerated samples is caused by differences in how sulfur atoms are bound to the $NiAl_2O_4$ surface. Sulfur content is measured by integrating the curve generated by the experiment, and because the peak from the used adsorbent is broadly distributed, it is lost into the background.

It is hypothesized that during the air regeneration step, the adsorbed benzothiophene is reacting with nickel to form NiS. In comparison to the used adsorbent, air regenerated samples showed a large, narrow peak which indicates sulfur bound in a single form. The formation of NiS during the air regeneraton step meant that only a faction of the original nickel sites were available for sulfur adsorption when exposed to fuel for a second time. As a result, the air regeneration process was not effective.

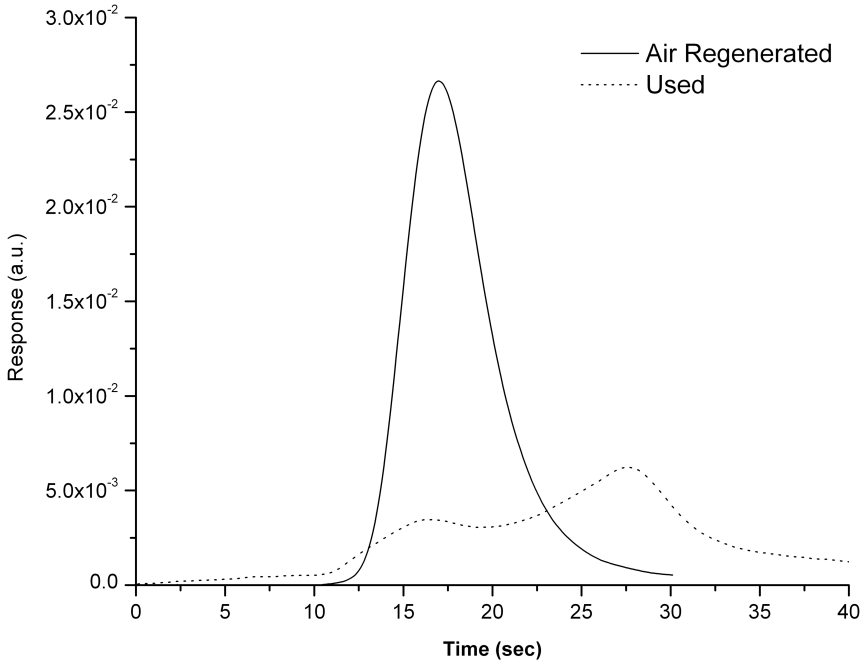

Fig. 29: IGA of unused and air regenerated adsorbent.

Overall, $NiAl_2O_4$ regenerates poorly as an adsorbent, likely do to the fact that not all the sulfur adsorbed is oxidized during regeneration. Longer regeneration times may improve performance, but regenerability will need to be improved significantly if $NiAl_2O_4$ is to be used efficiently.

4.4 Optimization of $NiAl_2O_4$ Activation and Adsorption Conditions

The primary goal of this project was to develop a material that achieved the deep desulfurization of fuels with the presumption that it would be used in a military application for on-site sulfur removal. Consequently, it is important that reduction times and temperatures be minimized to reduce the amount of energy and H_2 consumed during the process. Furthermore, a reduction of the reactor temperature during the desulfurization process is important for similar reasons. In this section the results

obtained by varying H_2 reduction time and temperature as well as an investigation of how sulfur capacity changes with reactor temperature are presented

In chemical adsorption processes, an increase in desulfurization capacity is expected when temperature is increased due to a reduction in the ability of physisorbed species to block active surface sites. When the temperature of the reactor was 50˚C and 100˚C, the desulfurization capacities were measured to be 0.4 and 0.6 ml-fuel per gram-adsorbent, respectively (fig. 30). When the temperature inside the reactor was increased to 150˚C, there was an increase in capacity to 3.4 ml-fuel per g-adsorbent.

It is most likely that moisture in the model fuel preferentially adsorbs to the nickel catalyst at temperatures below 100˚C, but desorbs at higher temperatures, leading to the significant capacities at a reactor temperature of 150˚C. The results of this experiment show that the reactor temperature must remain high, but is limited to the boiling point of the fuel (216˚C). As a result, a high capacity, room temperature desulfurization process using $NiAl_2O_4$ was not possible.

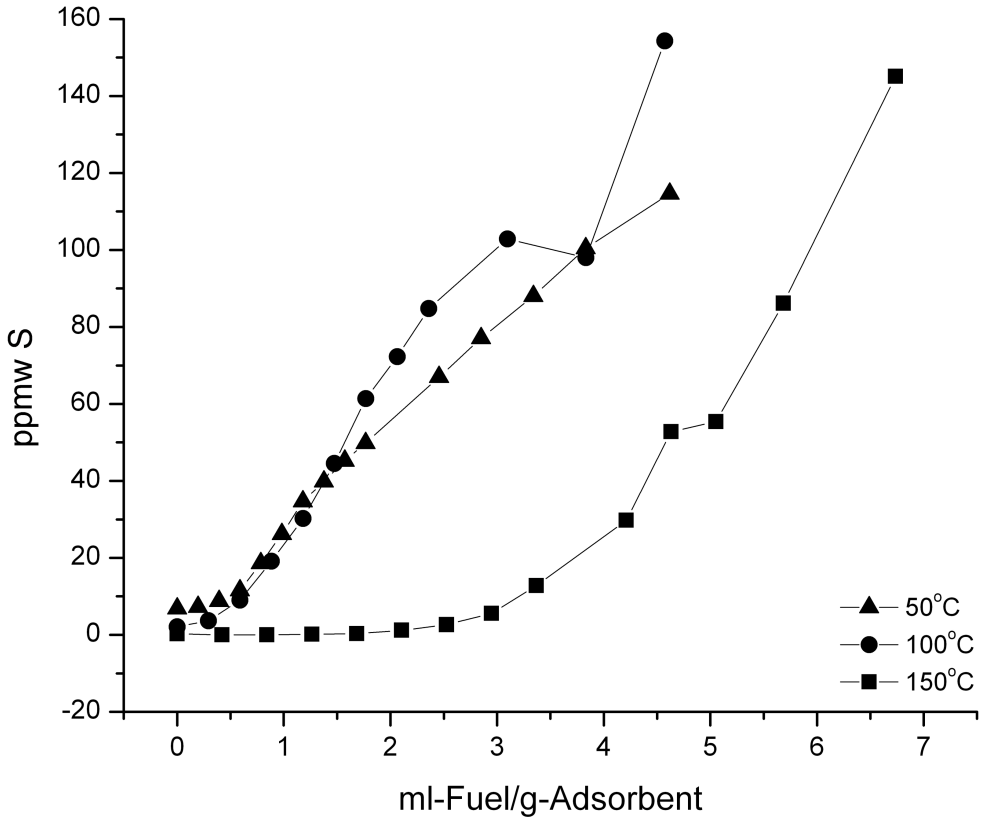

Fig. 30: Fixed-bed adsorption experiments completed at reactor temperatures of 50˚C, 100˚C, and 150˚C.

Once the reactor temperature was optimized, the effect of reduction temperature on capacity was investigated. $NiAl_2O_4$ pellets were reduced for 3 hours under H_2 at 200˚C, 300˚C, 400˚C, 500˚C, and 600˚C. The results of fixed-bed adsorption experiments conducted afterwards are presented in figure 31. Reduction temperature had a strong effect on the desulfurization capacity. This behavior is expected considering that the reduction of NiO to nickel increases enthalpy and entropy (ΔH, $\Delta S>0$). As such, increasing temperature increases driving "force" for the forward reaction. The increased reaction rate creates more nickel sites for benzothiophene to adsorb onto, which leads to an increase in sulfur capacity.

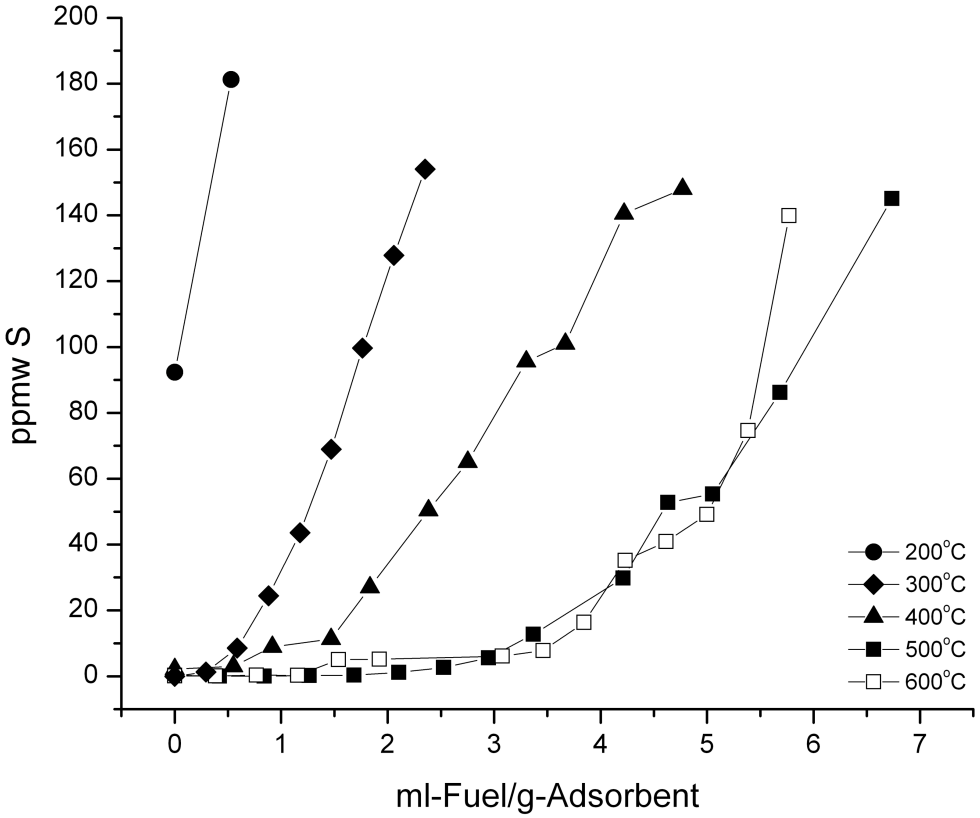

Fig. 31: The results of $NiAl_2O_4$ reduction for 3 hours at 200˚C, 300˚C, 400˚C, 500˚C, and 600˚C.

Capacity leveled off at reduction treatments with temperatures higher than 500˚C as shown in figure 32, and it is concluded that most of the reducible nickel is reacted after 3 hours at 500˚C, after which, no more adsorption sites are added by increasing the reduction temperature.

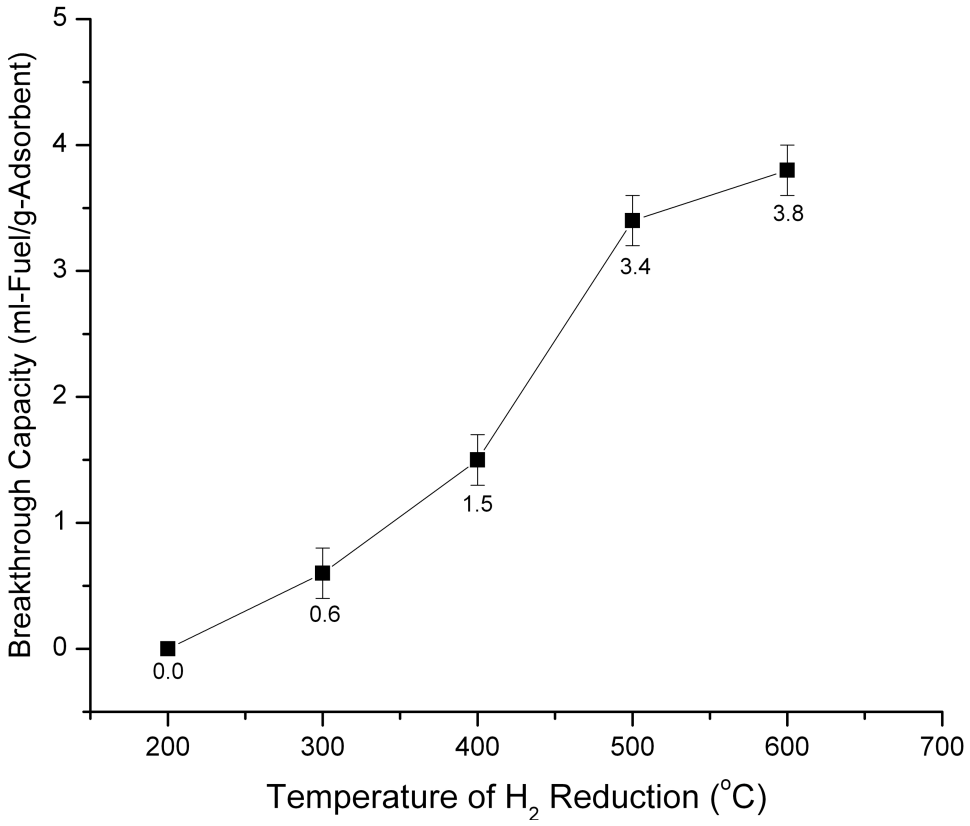

Fig. 32: The desulfurization capacity of $NiAl_2O_4$ plateaus at higher temperature treatments.

TGA of the reduction (fig. 33) showed four regions as temperature increased and provided insight into the capacity behavior shown previously. From room temperature to 350˚C physisorbed species are removed and the NiO is slowly reduced. A small drop in the weight by 0.6% between 350˚C and 440˚C is evidence of the reduction of NiO at the surface. After reduction at temperatures greater than 400˚C, the desulfurization capacity increased by a factor of 2.3. Between 440˚C and 650˚C, the weight of $NiAl_2O_4$ remains largely unchanged which helps to explain why capacity did not improve significantly at higher temperature reductions. These results are similar to a study by Murthy et al. on the effects of H_2 treatment on $NiAl_2O_4$.[57]

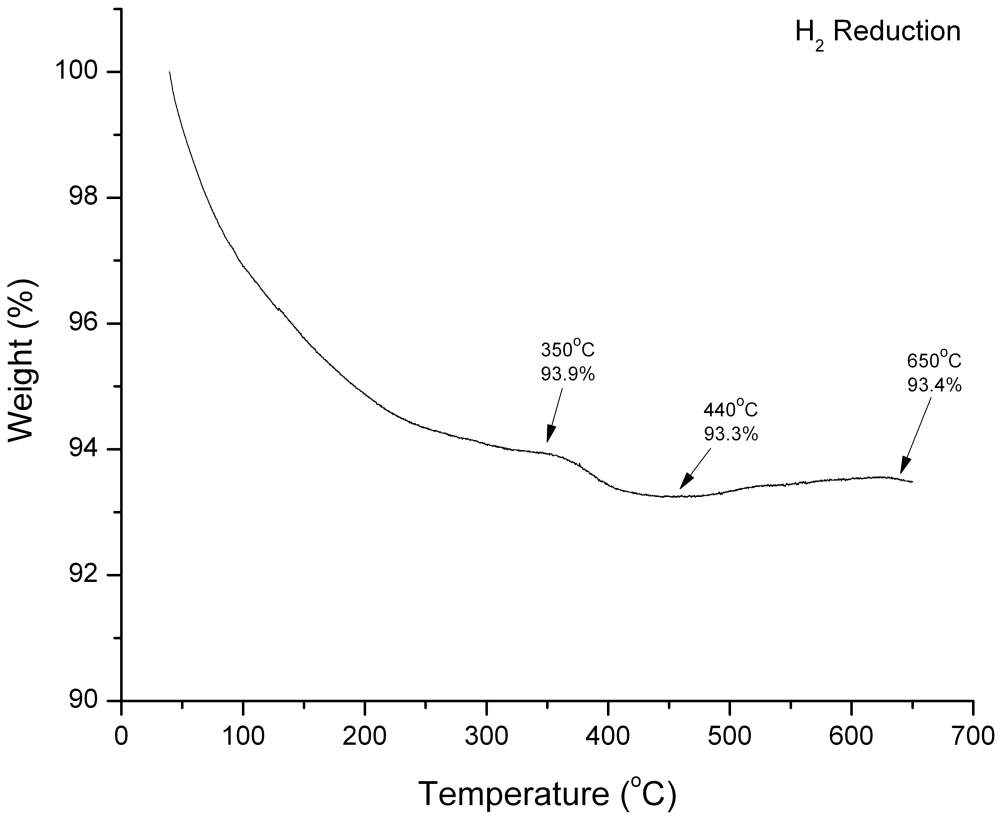

Fig. 33: TGA analysis of the H_2 reduction of $NiAl_2O_4$.

The optimal reduction temperature was chosen to be 500˚C due to the observed minor difference in desulfurization capacity between $NiAl_2O_4$ reduced for 3 hours at 500˚C and at 600˚C as well as the desire to operate at lower temperatures and minimize the amount of H_2 used in the process. From figures 34 and 35, it is apparent that at 500˚C, reduction for 3 hours yields the most significant capacity. When the adsorbent is reduced for 1 hour, it is able clean 1.95 ml-fuel per g-adsorbent to less than 15 ppmw S, and when reduced for 2 hours, capacity increased to 2.1 ml-fuel per g-adsorbent.

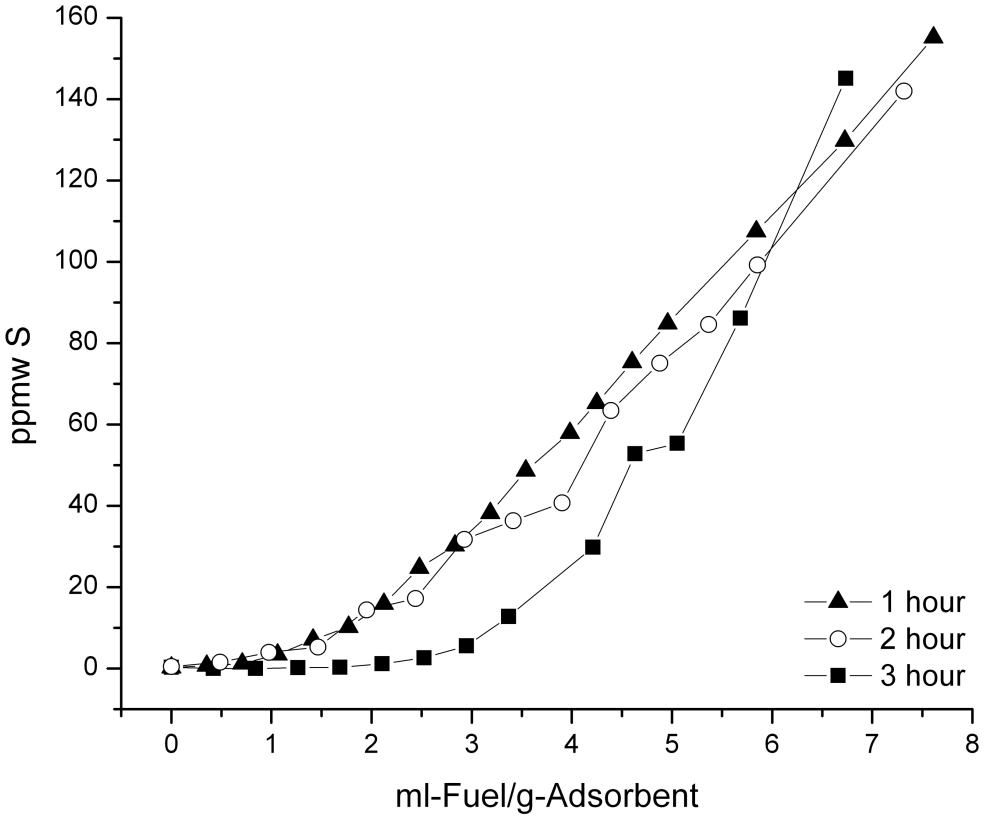

Fig. 34: Breakthrough curves from 1, 2, and 3 hour reductions at a constant temperature of 500˚C.

From these results, a reduction temperature of 500˚C for 3 hours and a reactor temperature of 150˚C maximize the amount of fuel that can be purified to less than 15 ppmw S while minimizing the cost and energy needed. The results of the entire study are tabulated below (table 8) with capacities divided between sub-ppmw sulfur levels and the EPA limit of 15 ppmw sulfur. Also included are the capacities of the H_2 and air regenerated adsorbents. Molar capacities of sulfur were calculated using equation 1 described previously.

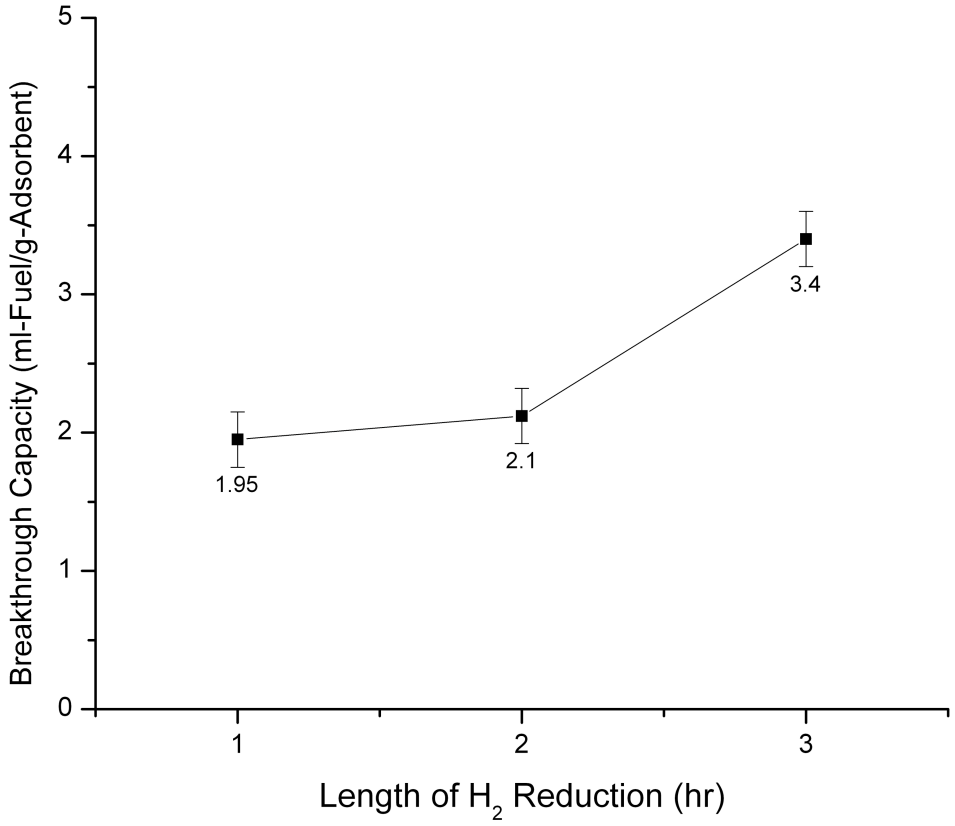

Fig. 35: Desulfurization capacity versus reduction time.

Table 8. Sulfur capacity of materials and conditions tested

Experimental Conditions		Sulfur Capacity (< 1 ppmw S)		Sulfur Capacity (< 15 ppmw S)	
Reduction Temperature	Reduction Time	ml-Fuel/g-Adsorbent	μmol-S/g-Adsorbent	ml-Fuel/g-Adsorbent	μmol-S/g-Adsorbent
200	3	--	--	--	--
300	3	0.29	1.5	0.6	4.8
400	3	0.55	4.1	1.5	12
500	3	2.1	14.5	3.4	23
600	3	1.5	10.2	3.8	23
500	2	0.7	4.8	2.1	14
500	1	0.5	3.4	1.95	13
Air Regeneration		0.35	2.4	1.4	9.3
H_2 Regeneration		0.57	3.5	0.90	5.7

CHAPTER 5

CONCLUSIONS AND RECOMMENDATIONS

Nanopowder $NiAl_2O_4$ was able to provide fuels with sulfur concentrations reduced to less than 15 ppmw. The advantages of using $NiAl_2O_4$ are both the ease in scalability of the synthesis and desulfurization processes. However, its relatively small capacity and sub-par regenerability when compared to zeolites make it a poor choice overall.

$NiAl_2O_4$ was synthesized by CCVC with an average crystallite size less than 12 nm. A 500˚C reduction for 3 h is required to achieve deep desulfurization of 3.4 ml of fuel per gram of $NiAl_2O_4$. Sintering of the nanopowders did not appear to become an issue in this study despite repeated heat treatments of pellet preparation, reduction, and regeneration. However, the ability of $NiAl_2O_4$ to be regenerated in air and hydrogen was limited. Other regeneration techniques or higher air regeneration temperatures for a longer period of time are necessary.

What became apparent in the course of this project was that pellets are not an ideal and efficient form for the nanopowders. While it stops the powders from becoming fluidized and obstructing the reactor downstream, the specific surface area of $NiAl_2O_4$ can be improved to allow even more contact between the adsorbent and the fuel. The next logical step in this regard is to attempt to either use CCVC to directly deposit a monolayer of powder on a high surface area substrate. Similarly, the synthesized powders could be deposited via dip-coating or some other technique onto a large surface area support structure. This would serve to minimize the amount of adsorbent needed in the

reactor to achieve the same level of desulfurization because more nickel sites will come in contact with the fuel.

Furthermore, H_2 reduction is costly and not ideal for the development of an adsorptive material. It must be removed or severely reduced for $NiAl_2O_4$ to become a viable alternative. The primary objective for the deep desulfurization of jet fuel is not only so JP-8 can be used in all military vehicles, but so it can then be broken down into low-sulfur H_2 for fuel cells in the field. Hydrogen reduction steps diminish the efficiency of this process. Therefore it is more important to investigate a different desulfurization mechanism that does require reduced metals at the surface. As mentioned in the literature review, a thermovacuum treatment has been reported to create oxygen vacancies $ZnAl_2O_4$ that adsorbent thiophene in a model fuel. In addition, nickel was reduced in $NiAl_2O_4$ in miniscule amounts, and much of the adsorbent surface area is left inactive. A surface activation treatment to create sites that are slightly acidic in character could also serve to increase capacity and perhaps allow for room temperature adsorption.

The regeneration of $NiAl_2O_4$ proved to be problematic in this study, which is another reason to move away from this particular material. Coking and the loss of nickel sites to NiS became the reason for deactivation. Further investigation of heating treatments to oxidize more sulfur without surface area loss or modifications could improve regenerability.

APPENDIX

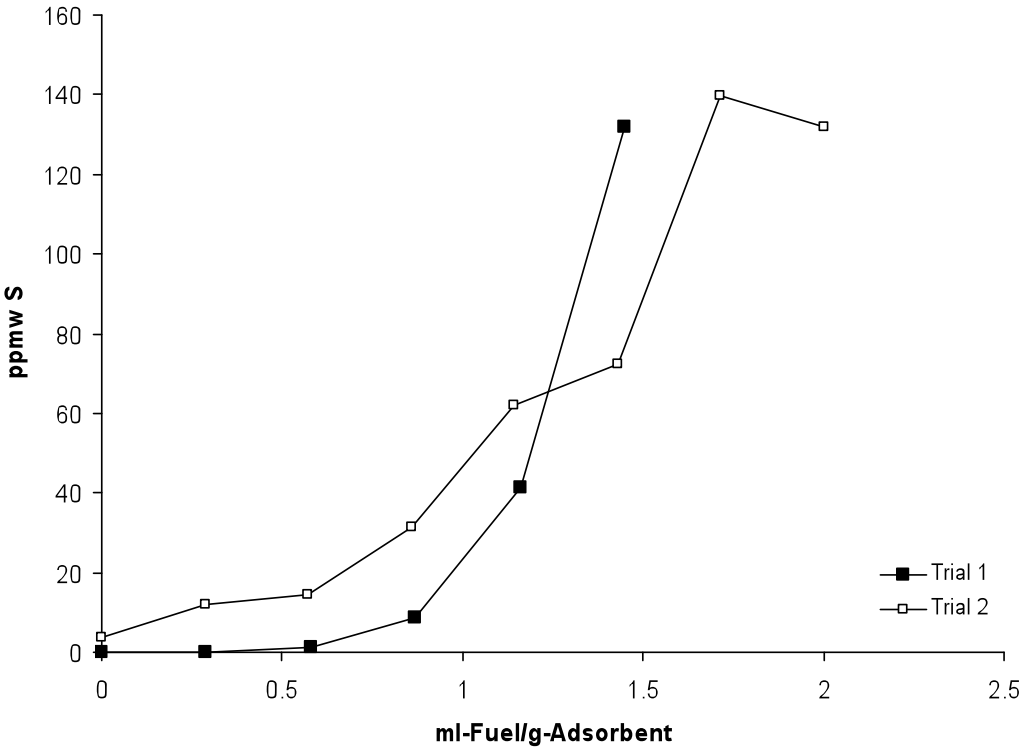

Fig. 36: Reduction in H_2 for 3 hours at 500˚C followed by H_2 regeneration step.

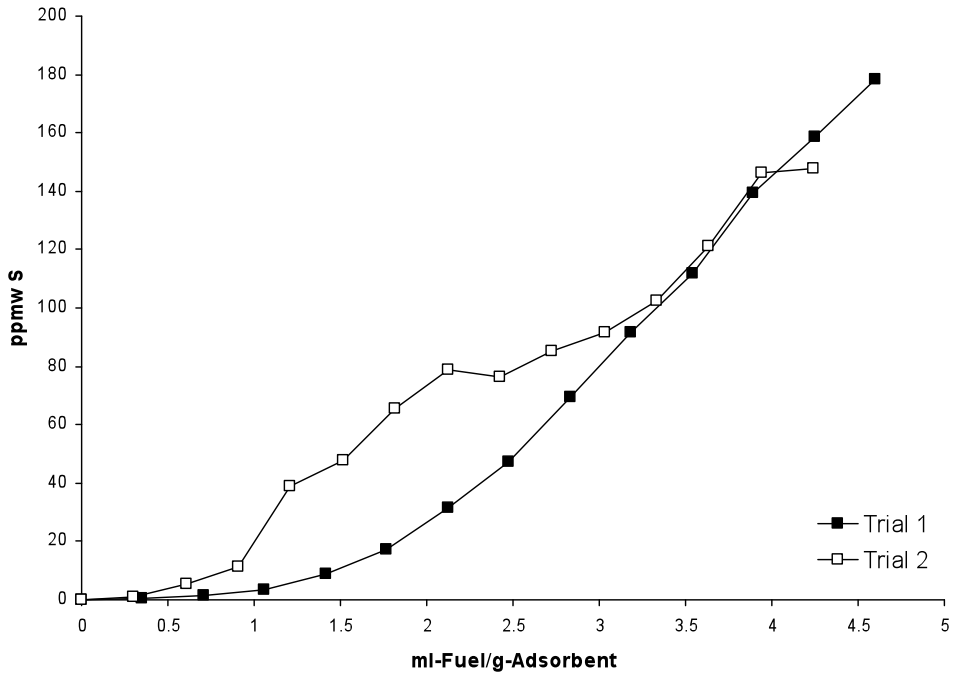

Fig. 37: Reduction in H_2 for 3 hours at 500˚C followed by an air regeneration step, then H_2 reduction.

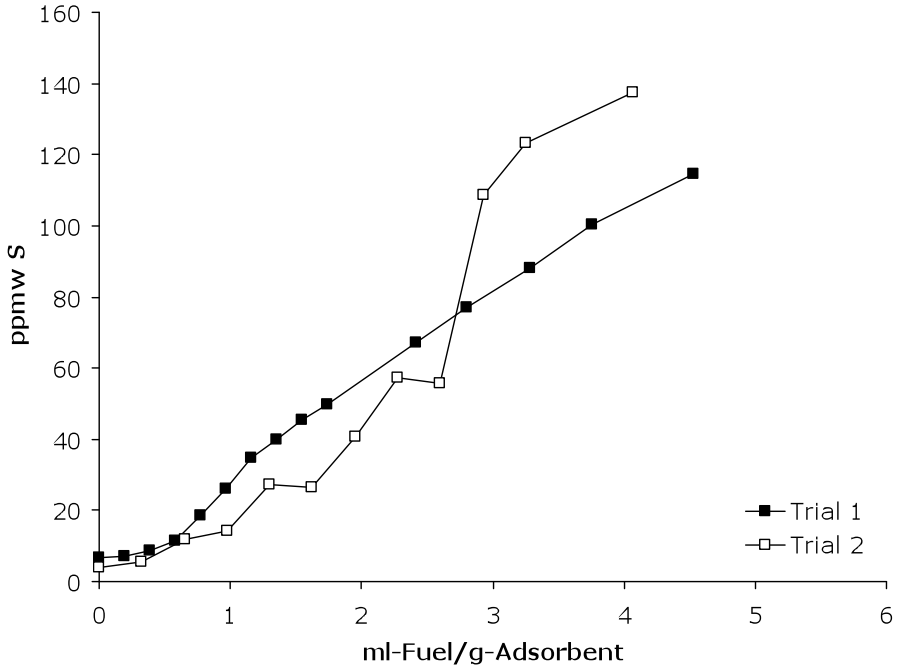

Fig. 38: Reduction in H_2 for 3 hours at 500˚C, then an adsorption experiment at 50˚C.

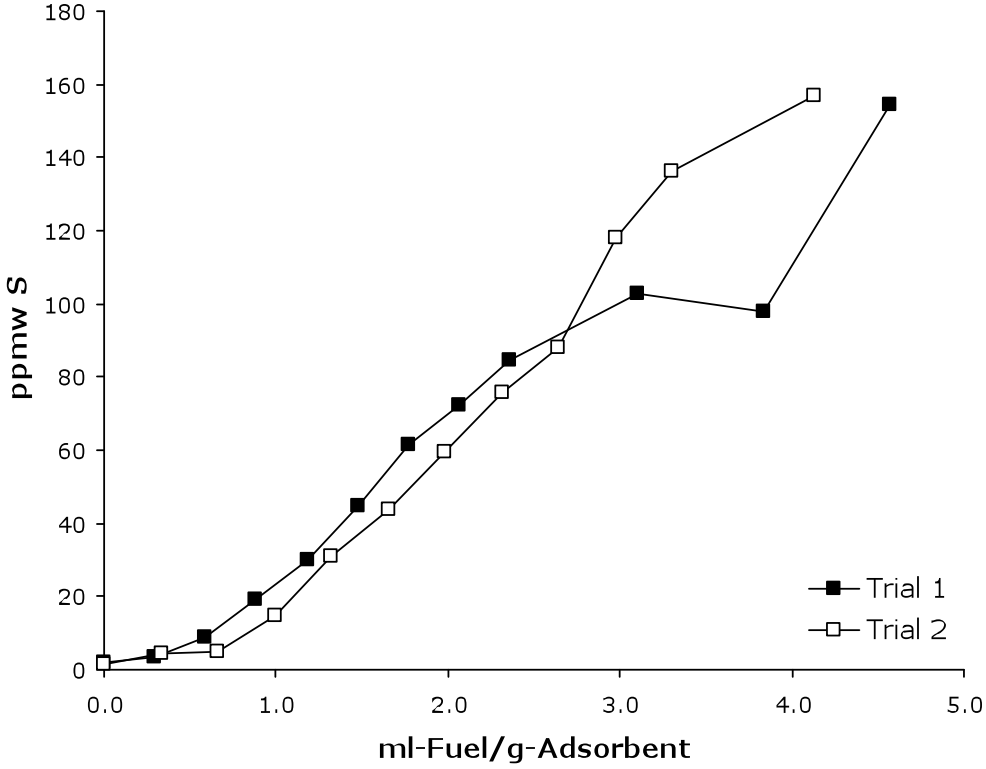

Fig. 39: Reduction in H_2 for 3 hours at 500˚C, then an adsorption experiment at 100˚C.

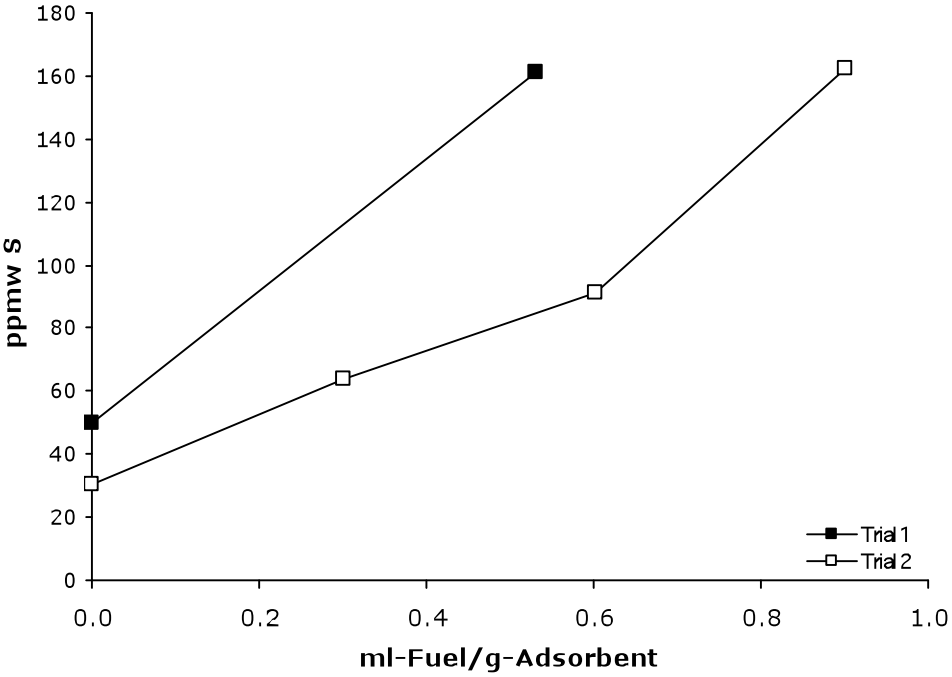

Fig. 40: Reduction in H_2 for 3 hours at 200˚C.

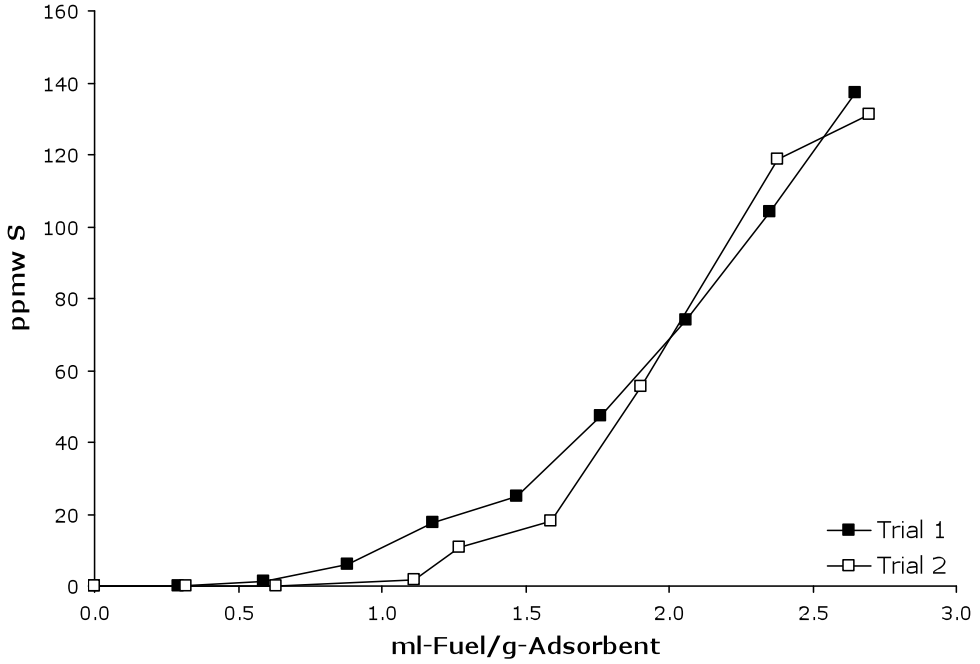

Fig. 41: Reduction in H_2 for 3 hours at 300˚C.

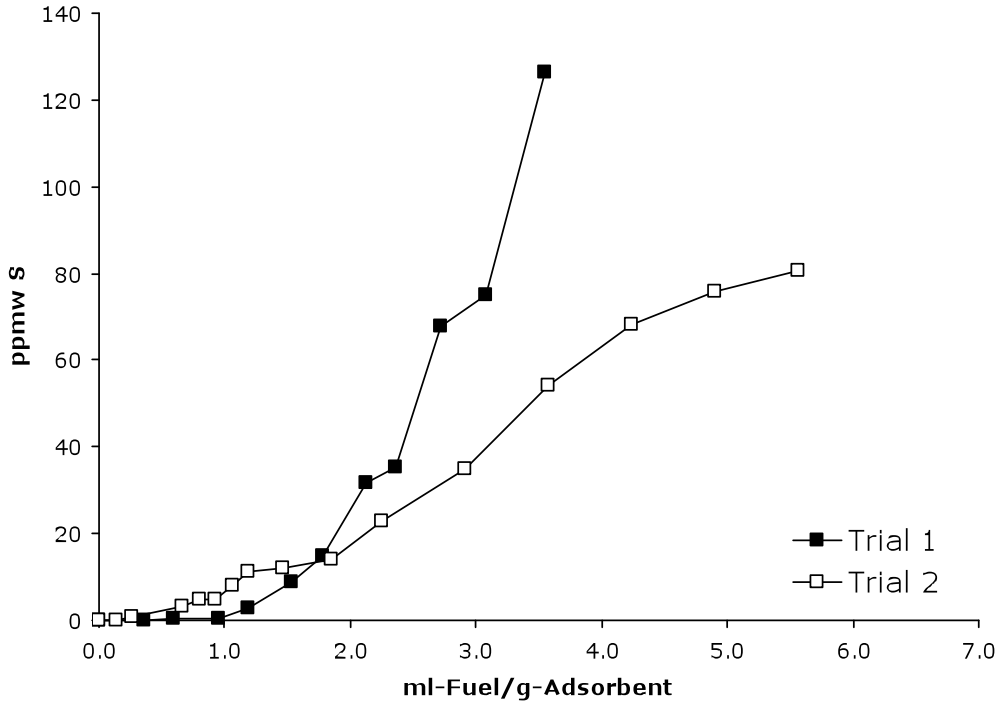

Fig. 42: Reduction in H_2 for 3 hours at 400˚C.

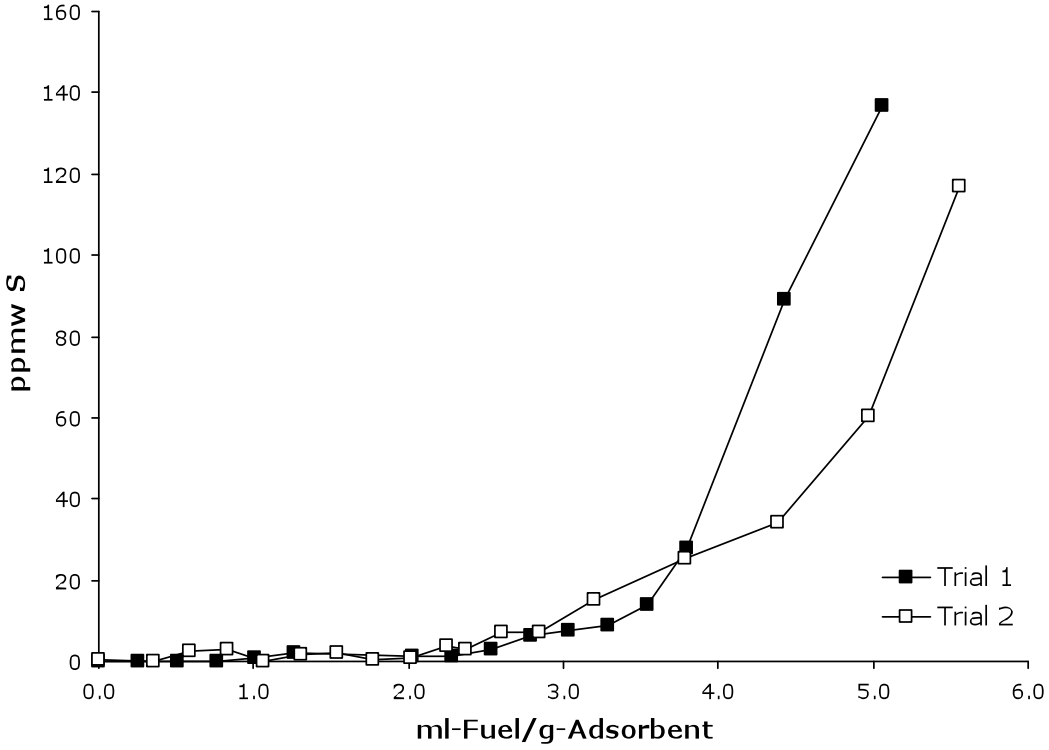

Fig. 43: Reduction in H_2 for 3 hours at 600˚C.

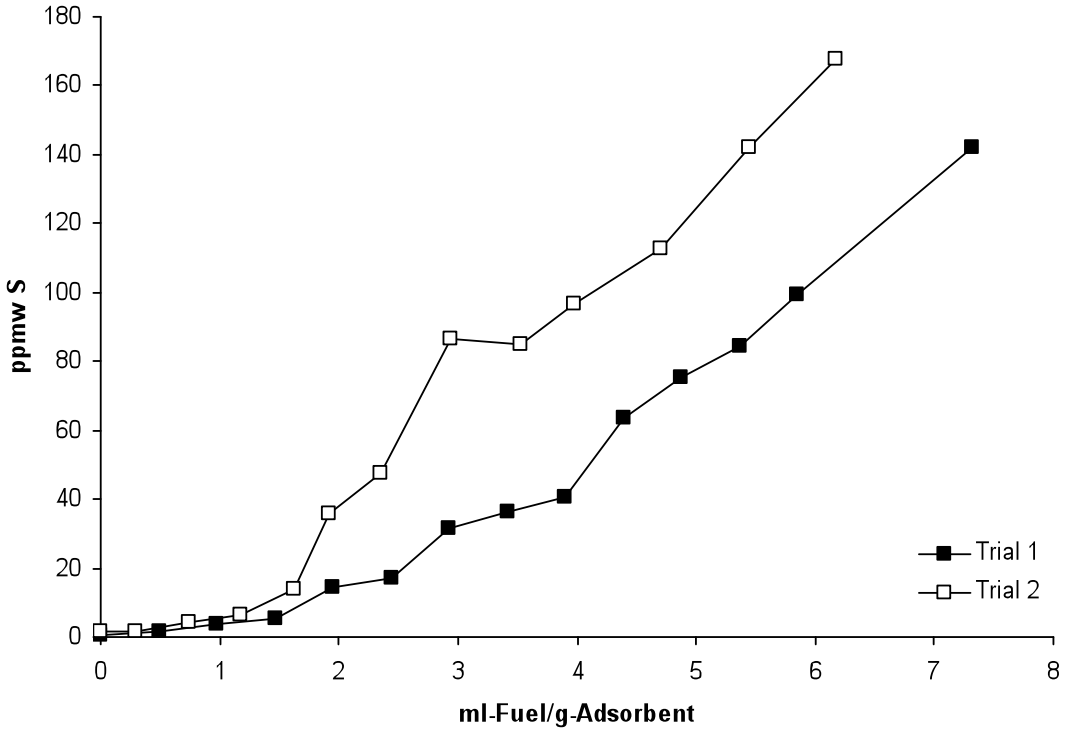

Fig. 44: Reduction in H_2 for 1 hour at 500˚C.

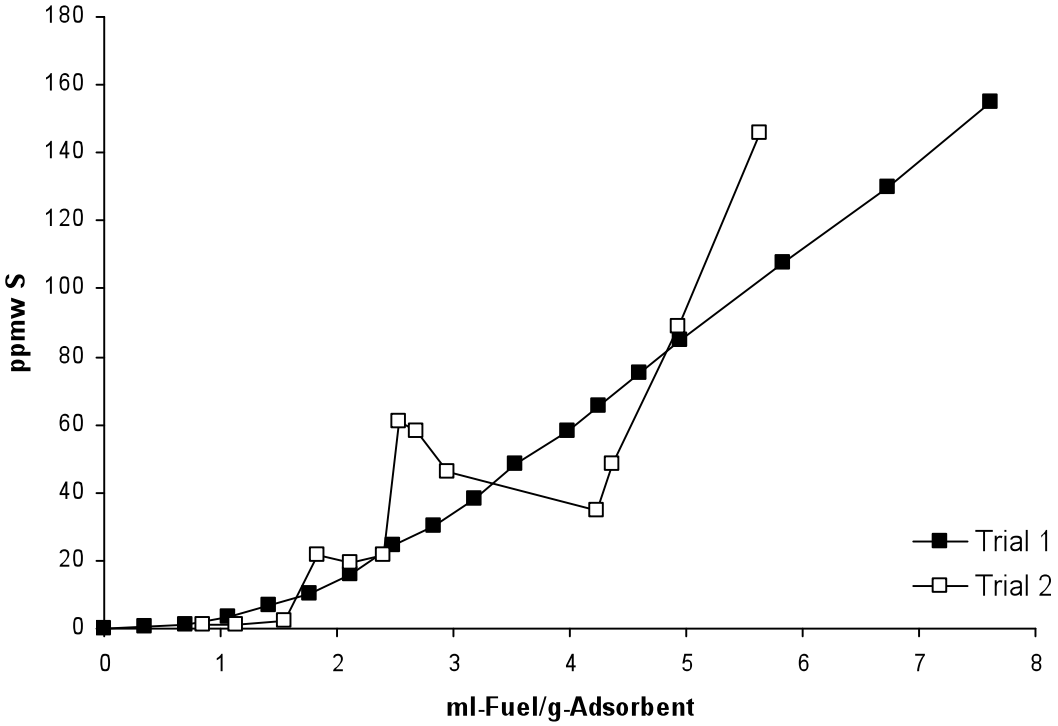

Fig. 45: Reduction in H_2 for 2 hours at 500˚C.

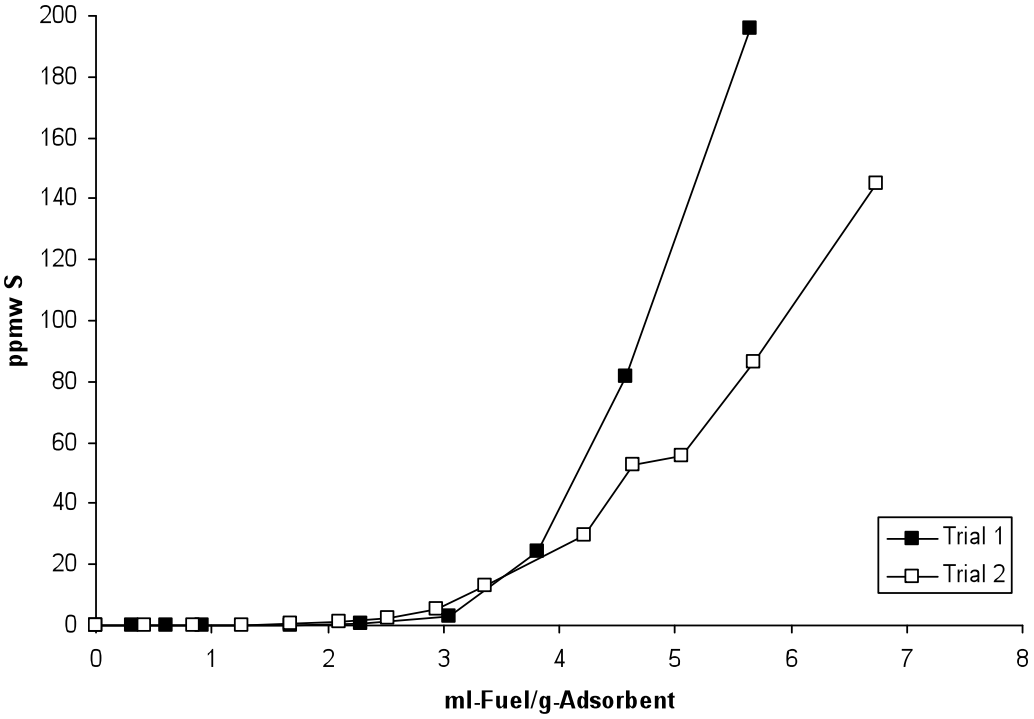

Fig. 46: Reduction in H_2 for 3 hours at 500˚C.

REFERENCES

[1] M. Breysse, G. Djega-Mariadassou, S. Pessayre, C. Geantet, M. Vrinat, and G. Perot, *Deep desulfurization: Reactions, catalysts and technological challenges.* Catalysis Today, **84**, (2003): 129.

[2] C. Song and X. Ma, *New design approaches to ultra-clean diesel fuels by deep desulfurization and deep dearomatization.* App. Catal. B, **41**, (2003): 207.

[3] S. Velu, X. Ma, and C. Song, *Selective adsorption for removing sulfur from jet fuel over zeolite-base adsorbents.* Ind. Eng. Chem. Res., **42**, (2003): 5293.

[4] C. Song, *An overview of new approaches to deep desulfurization for ultra-clean gasoline, diesel and jet fuel.* Catalysis Today, **86**, (2003): 211.

[5] T. Edwards, *System drivers for high heat sink fuels.* Am. Chem. Soc. Div. Petrol. Chem. Prepr., **45**, (2000): 436.

[6] J.H. Kim, X. Ma, A. Zhou, and C. Song, *Ultra-deep desulfurization and denitrogenation of diesel fuel by selective adsorption over three different adsorbents: A study on adsorptive selectivity and mechanism.* Catalysis Today, **111**, (2006): 74.

[7] M. Jiang and F.T.T. Ng, *Adsorption of benzothiophene on Y zeolites investigated by infrared spectroscopy and flow calorimetry.* Catalysis Today, **116**, (2006),(530-536)

[8] X. Ma, M. Sprague, and C. Song, *Deep desulfurization of gasoline by selective adsorption over nickel-based adsorbent for fuel cell applications.* Ind. Eng. Chem. Res., **44**, (2005): 5768.

[9] A.J. Hernandez-Maldonado, F.H. Yang, G. Qi, and R.T. Yang, *Desulfurization of transportation fuels by π-complexation sorbents: Cu(I)-, Ni(II)-, and Zn(II)-zeolites.* App. Catal. B, (2005),(41): 111.

[10] V. Ukkirapandian, V. Sadasivam, and B. Sivasankar, *Oxidation of dibenzothiophene and desulphurization of diesel.* Petroleum Science and Technology, **26**, (2008),(4): 423.

[11] J.T. Sampanthar, H. Xiao, J. Dou, T.Y. Nah, X. Rong, and W.P. Kwan, *A novel oxidative desulfurization process to remove refractory sulfur compounds from diesel fuel.* Applied Catalysis B: Environmental, **63**, (2006): 85.

[12] M. Soleimani, A. Bassi, and A. Margaritis, *Biodesulfurization of refractory organic sulfur compounds in fossil fuels.* Biotechnology Advances, **25,** (2007): 570.

[13] I.V. Babich and J.A. Moulijin, *Science and technology of novel processes for deep desulfurization of oil refinery streams: A review.* Fuel, **82**, (2003): 607.

[14] J. Goering and U. Burghaus, *Adsorption kinetics of thiophene on single-walled carbon nanotubes (CNTs).* Chemical Physics Letters, **447**, (2007),(1-3): 121.

[15] A. Takahashi, F.H. Yang, and R.T. Yang, *New sorbents for desulfurization by π-complexation: Thiophene/benzene adsorption.* Ind. Eng. Chem. Res., **41**, (2002): 2487.

[16] A.P. Singh, P.C. Singh, and V.N. Singh, Ind. Eng. Chem. Res., **27**, (1988): 2101.

[17] V.M. Bhandari, C.H. Ko, J.G. Park, S.-S. Han, S.-H. Cho, and J.-N. Kim, *Desulfurization of diesel using ion-exchanged zeolites.* Chemical Engineering Science, **61**, (2006): 2599.

[18] A.J. Hernandez-Maldonado and R.T. Yang, *Desulfurization of commercial jet fuels by adsorption via π-complexation with vapor phase ion exchanged Cu(I)-Y zeolites.* Ind. Eng. Chem. Res., **43**, (2004): 6142.

[19] A.J. Hernandez-Maldonado and R.T. Yang, *Desulfurization of diesel fuels by adsorption via π-complexation with vapor-phase exchanged Cu(I)-Y zeolites.* J. Am. Chem. Soc., **126**, (2004): 992.

[20] R.M. Cole and D.D. Davidson, *Hydrodesulfurization of gasoline fractions with tungsten–nickel sulfide catalyst.* Industrial & Engineering Chemistry, **41**, (1949): 2711.

[21] A.C. Byrns, W.E. Bradley, and M.W. Lee, *Catalytic desulfurization of gasolines by cobalt molybdate process.* Industrial & Engineering Chemistry, **35**, (1943): 1160.

[22] R.M. Casagrande, W.K. Meerbott, and R.P. Trainer, *Selective hydrotreating over tungsten nickel sulfide catalyst.* Industrial & Engineering Chemistry, **47**, (1955): 744.

[23] M. Daage and R.R. Chianelli, *Structure-function relations in molybdenum sulfide catalysts: The rim-edge model.* J. Catal., **194**, (1994): 414.

[24] E. Ito and J.A.R.v. Veen, *On novel processes for removing sulphur from refinery streams.* Catalysis Today, **116**, (2006): 446.

[25] M.J. Girgis and B.C. Gates, *Reactivities, reaction networks, and kinetics in high-pressure catalytic hydroprocessing.* Ind. Eng. Chem. Res., **30**, (1991): 2021.

[26] N.K. Nag, A.V. Sapre, D.H. Broderick, and B.C. Gates, *Hydrodesulfurization of polycyclic aromatics catalyzed by sulfided CoO---MoO_3/γ-Al_2O_3: The relative reactivities.* Journal of Catalysis, **57**, (1979): 509.

[27] M. Houalla, D.H. Broderick, A.V. Sapre, N.K. Nag, V.H.J.d. Beer, B.C. Gates, and H. Kwart, *Hydrodesulfurization of methyl-substituted dibenzothiophenes catalyzed by sulfided Co---Mo/γ-Al_2O_3.* Journal of Catalysis, **61**, (1980): 523.

[28] D.D. Whitehurst, T. Isoda, and I. Mochida, Advanced Catalysis, **42**, (1998): 362.

[29] X. Ma, K. Sakanishi, and I. Mochida, *Hydrodesulfurization reactivities of various sulfur compounds in diesel fuel.* Ind. Eng. Chem. Res., **33**, (1994),(218-222)

[30] S. Romanow-Garcia, *Cleaner fuel -- it's just not that simple.* Hydrocarbon Process, **79**, (2000): 17.

[31] P. Jeevanandam, K.J. Klabunde, and S.H. Tetzler, *Adsorption of thiophenes out of hydrocarbons using metal impregnated nanocrystalline aluminum oxide.* Microporous and Mesoporous Materials, **79**, (2005): 101.

[32] C. Yu, J. Qiu, Y. Sun, X. Li, G. Chen, and Z. Zhao, *Adsorption removal of thiophene and dibenzothiophene from oils with activated carbon as adsorbent: Effect of surface chemistry.* Journal of Porous Materials, **15**, (2008),(2): 151.

[33] H.Y. Zhang, G.B. Shan, H.Z. Liu, and J.M. Xing, *Surface modification of γ-Al_2O_3 nano-particles with gum arabic and its applications in adsorption and biodesulfurization.* Surface and Coatings Technology, **201**, (2007): 6917.

[34] A.B.S.H. Salem, *Naphtha desulfurization by adsorption.* Industrial & Engineering Chemistry Research, **33**, (1994): 336.

[35] A.B.S.H. Salem and H.S. Hamid, *Removal of sulfur compounds from naphtha solutions using solid adsorbents.* Chemical Engineering & Technology, **20**, (1997): 342.

[36] C.O. Ania and T.J. Bandosz, *Importance of structural and chemical heterogeneity of activated carbon surfaces for adsorption of dibenzothiophene* Langmuir, **21**, (2005): 7752.

[37] J. Cejka, *Introduction to zeolite molecular sieves*. 2007, Amsterdam: Elsevier.

[38] J. Weitkamp, M. Schwark, and S. Ernest, *Removal of thiophene impurities from benzene by selective adsorption in zeolite ZSM-5.* Journal of the Chemical Society. Chemical communications, (1991): 1133.

[39] F.T.T. Ng, A. Rahman, T. Ohasi, and M. Jiang, *A study of the adsorption of thiophenic sulfur compounds using flow calorimetry.* Applied Catalysis B: Environmental, **56**, (2005): 127.

[40] Y. Li, F.H. Yang, G. Qi, and R.T. Yang, *Effects of oxygenates and moisture on adsorptive desulfurization of liquid fuels with Cu(I)Y zeolite.* Catalysis Today, **116**, (2006): 512.

[41] A.J. Hernandez-Maldonado, S.D. Stamatis, and R.T. Yang, *New sorbents for desulfurization of diesel fuels via π-complexation: Layered beds and regeneration.* Ind. Eng. Chem. Res., **43**, (2004): 769.

[42] K.J. Klabunde, J. Stark, O. Koper, C. Mohs, D.G. Park, S. Decker, Y. Jiang, I. Lagadic, and D. Zhang, *Nanocrystals as stoichiometric reagents with unique surface chemistry.* J. Phys. Chem., **100**, (1996),(30): 12142.

[43] C.H. Ko, J.G. Park, J.C. Park, H. Song, S.-S. Han, and J.-N. Kim, *Surface status and size influences of nickel nanoparticles on sulfur compound adsorption.* Applied Surface Science, **253**, (2007),(13): 5864.

[44] X. Yang, C. Cao, K.J. Klabunde, K.L. Hohn, and L.E. Erickson, *Adsorptive desulfurization with xerogel-derived zinc-based nanocrystalline aluminum oxide.* Ind. Eng. Chem. Res., **46**, (2007),(14): 4819.

[45] A.T. Hunt, W.B. Carter, and J. J. K. Cochran, *Combustion chemical vapor depostion: A novel thin-film deposition technique.* Appl. Phys. Lett., **63**, (1993): 266.

[46] R. Maric, M. Oljaca, B. Vukasinovic, and A.T. Hunt, *Synthesis of oxide nanopowders in nanospray diffusion flames.* Materials and Manufacturing Processes, **19**, (2004),(6): 1143.

[47] N.M. Galea, E.S. Kadantsev, and T. Ziegler, *Studying reduction in solid oxide fuel cell activity with density fuctional theory effects of hydrogen sulfide adsorption on Ni anode surface.* Journal of Physical Chemistry C, **111**, (2007): 14457.

[48] J.D. Seader, E.j. Henley. *Separation process principles*. New York: Wiley; 1998.

[49] B.D. Cullity and S.R. Stock, *Elements of x-ray diffraction*. 3rd ed. 2001, Upper Saddle River, N.J.: Prentice Hall.

[50] J.A. Azurdia, J. Marchal, P. Shea, H. Sun, X.Q. Pan, and R.M. Laine, *Liquid-feed flame spray pyrolysis as a method of producing mixed-metal oxide nanopowders of potential interest as catalytic materials. Nanopowders along the NiO-Al_2O_3 tie line including $(NiO)_{0.22}(Al_2O_3)_{0.78}$, a new inverse spinel composition.* Chem. Mater., **18**, (2006),(3): 731.

[51] H. Furuhashi, M. Inagaki, and S. Naka, *Determination of cation distribution in spinels by x-ray diffraction method.* Journal of Inorganic and Nuclear Chemistry, **35**, (1973): 3009.

[52] Y.S. Han, J.B. Li, X.S. Ning, X.Z. Yang, and B. Chi, *Study on NiO excess in preparing $NiAl_2O_4$.* Materials Science and Engineering A, **369**, (2004),(1-2): 241.

[53] G. Kresse and J. Hafner, *First-principles study of the adsorption of atomic H on Ni(111), (100) and (110).* Surface Science, **459**, (2000),(3): 287.

[54] J.F. Moulder, J. Chastain, and R.C. King, *Handbook of x-ray photoelectron spectroscopy : A reference book of standard spectra for identification and interpretation of XPS data*. 1995, Eden Prairie, Minn.: Physical Electronics.

[55] R.B. Shalvoy and P.J. Reucroft, *Characterization of a sulfur-resistant methanation catalyst by XPS.* J. Vac. Sci. Technol., **16**, (1979): 567.

[56] R.P. Furstenau, G. McDougall, and M.A. Langell, *Initial stages of hydrogen reduction of NiO(100).* Surf. Sci., **150**, (1985): 55.

[57] I. Murthy and C.S. Swamy, *Catalytic behavior of $NiAl_2O_4$ spinel upon hydrogen treatment.* Journal of Materials Science, **28**, (1993),(5): 1194.